

Quantum Computing and Tensor Networks for Laminate Design: A Novel Approach to Stacking Sequence Retrieval

Arne Wulff¹, Boyang Chen^{*1}, Matthew Steinberg², Yinglu Tang¹, Matthias Möller², and Sebastian Feld²

¹Faculty of Aerospace Engineering, Delft University of Technology, The Netherlands

²Faculty of Electrical Engineering, Mathematics and Computer Science, Delft University of Technology, The Netherlands

Abstract

As with many tasks in engineering, structural design frequently involves navigating complex and computationally expensive problems. A prime example is the weight optimization of laminated composite materials, which to this day remains a formidable task, due to an exponentially large configuration space and non-linear constraints. The rapidly developing field of quantum computation may offer novel approaches for addressing these intricate problems. However, before applying any quantum algorithm to a given problem, it must be translated into a form that is compatible with the underlying operations on a quantum computer. Our work specifically targets stacking sequence retrieval with lamination parameters, which is typically the second phase in a common bi-level optimization procedure for minimizing the weight of composite structures. To adapt stacking sequence retrieval for quantum computational methods, we map the possible stacking sequences onto a quantum state space. We further derive a linear operator, the Hamiltonian, within this state space that encapsulates the loss function inherent to the stacking sequence retrieval problem. Additionally, we demonstrate the incorporation of manufacturing constraints on stacking sequences as penalty terms in the Hamiltonian. This quantum representation is suitable for a variety of classical and quantum algorithms for finding the ground state of a quantum Hamiltonian. For a practical demonstration, we chose a classical tensor network algorithm, the DMRG algorithm, to numerically validate our approach. For this purpose, we derived a matrix product operator representation of the loss function Hamiltonian and the penalty terms. Numerical trials with this algorithm successfully yielded approximate solutions, while exhibiting a tradeoff between accuracy and runtime. Although this work primarily concentrates on quantum computation, the application of tensor network algorithms presents a novel quantum-inspired approach for stacking sequence retrieval.

Keywords: quantum computing, tensor networks, composite laminates, stacking sequence retrieval

1 Introduction

Across various engineering disciplines, researchers and practitioners regularly encounter complex and computationally intensive problems [1–3]. The rapidly evolving field of quantum computing could offer crucial breakthroughs in addressing these issues and exceed the capabilities of conventional methods [4–9]. As this technology continues to mature, the potential benefits it offers to complex engineering problems are becoming more apparent [10–22]. However, the challenge lies in accurately identifying those scenarios where quantum computing holds an advantage and in crafting algorithms to harness this potential. To address this, initiating the development of quantum algorithms for engineering applications now, in parallel with quantum hardware advancements, is essential. Such an approach positions us to immediately harness the full capabilities of quantum computing in engineering as soon as it becomes available.

The design of laminated composite materials [23, 24] is an example of a complex engineering challenge which could benefit from a quantum-based approach. These materials are extensively used in aerospace applications for their high strength-to-weight ratio. Furthermore, these materials consist of many

^{*}Corresponding author, b.chen-2@tudelft.nl

configurable layers, each impacting the overall stiffness. The stiffness characteristics of the whole material can therefore be tailored to the specific requirements of a structure [25, 26]. However, determining the optimal arrangement for specific applications from the exponentially large configuration space is a significant challenge, positioning laminated composites as a suitable candidate for quantum computing applications [27, 28].

A widely used method in designing composite structures involves a bi-level optimization procedure [29–35]. The initial phase focuses on optimizing the material’s thickness and stiffness characteristics, expressed through lamination parameters [36, 37]. Subsequently, the second phase involves finding a feasible stacking sequence that aligns with the lamination parameters determined earlier. While the first phase typically employs continuous gradient descent methods, the second stage, stacking sequence retrieval, constitutes an intricate combinatorial optimization problem, particularly when incorporating manufacturing considerations [38–41].

Optimizing stacking sequences for constant stiffness structures has been addressed through various methods, including layer-wise optimization [42, 43], branch-and-bound [35, 44–46] and beam search [47] techniques. The complexity increases substantially for structures that necessitate variable stiffness, often achieved by dividing the structure into distinct panels [48, 49], each requiring a specific stacking sequence and stiffness. Ensuring structural integrity by matching the stacking sequences across different panels, in accordance with blending rules [50–53], adds a further layer of complexity, and adapting the previously mentioned methods to this multi-panel scenario is challenging. Given this complexity, often intensified by the curse of dimensionality, current methods generally rely on meta-heuristics such as genetic algorithms [30–32, 34, 35, 54–56] or particle swarm optimization [56–58], which are frequently used in conjunction with problem-specific methods like stacking sequence tables [59, 60] to address these challenges. Despite this progress, the quest for more efficient solutions in stacking sequence retrieval remains a pivotal area of research, indicating the necessity for novel approaches in this complex domain. Quantum computing may offer a unique approach to manage these complex, high dimensional scenarios effectively. Nevertheless, the foundational work on single constant-stiffness panels must be established first.

In this work, we explore the adaptation of the *stacking sequence retrieval problem* (SSR) with lamination parameters for constant stiffness panels to quantum algorithms. Initially, we formalize the problem as an integer-optimization problem, suitable for translation into a quantum mechanics framework. This involves representing variable configurations of the problem as states in a Hilbert space and deriving a Hamiltonian to embody the problem’s loss function. The objective then becomes identifying the ground-state of the Hamiltonian, a task addressable by various quantum algorithms [6, 15, 61–71]. We also present how manufacturing constraints can be incorporated as penalty terms within the Hamiltonian. As a demonstration of our formalism, a numerical simulation is performed using the density matrix renormalization group algorithm (DMRG), a tensor network method effective in finding ground states of many-body systems [72–77]. For this purpose, the Hamiltonian must first be expressed in terms of a matrix product operator (MPO), which is a particular tensor network structure. This enables us to optimize systems as large as 200 plies, by controlling the bond dimension of the states’ MPS. We conducted tests under various conditions, including altering bond dimensions and sweeping directions, and factoring in a disorientation constraint. The optimization results successfully approximated the optimal solutions, validating our Hamiltonian construction and confirming the efficacy of our approach. Furthermore, the notable performance of the DMRG algorithm points to the potential of tensor network methods as a quantum-inspired alternative to conventional stacking sequence retrieval methods.

Following this introduction, section 2 begins with an overview of laminated composite materials and concludes with the formulation of the specific integer-optimization problem that we employ in the remainder of this work. In section 3, we map the problem to a quantum state space, and construct the Hamiltonian corresponding to the problem’s loss function. We additionally show how to integrate manufacturing constraints as penalty terms in the Hamiltonian. In section 4, after a brief introduction to tensor networks, we derive the Hamiltonian in MPO form. Section 5 presents the results of our numerical simulation, examining various testing conditions and parameters. The paper concludes with section 6, and summarizes our findings, as well as ramifications for the field of quantum computing in the context of engineering and materials science applications.

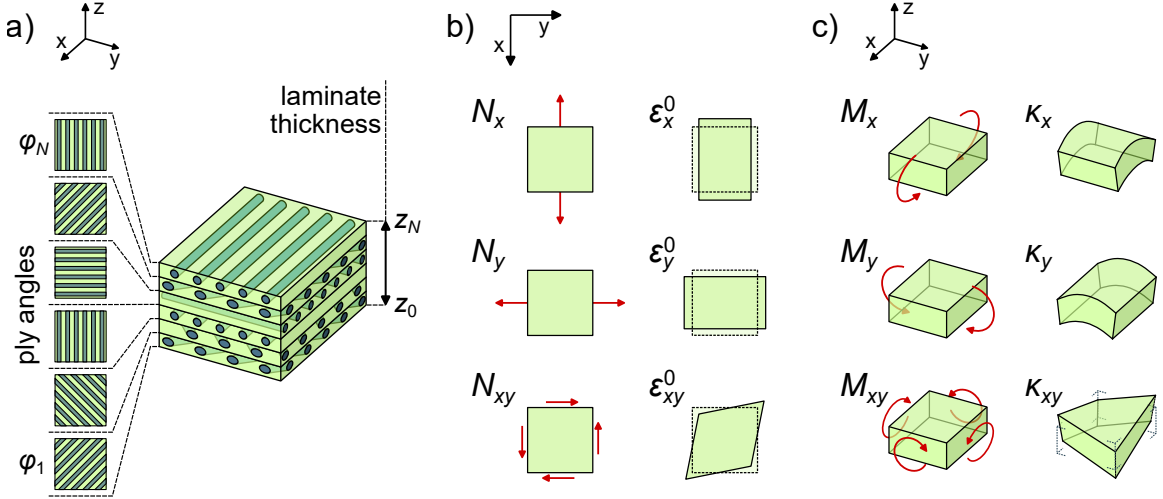


Figure 1: a) Diagram of a laminated composite material, which consists of multiple layers that are oriented in different directions. b) A representation of the stress resultants \vec{N} , which for isotropic materials result in in-plane deformations $\vec{\varepsilon}^0$. c) A pictographical representation of the moment resultants \vec{M} , which for isotropic materials result in out-of-plane bending $\vec{\kappa}$. Non-diagonal elements in the **ABD**-matrix allow for coupling between all possible stress and moment resultants on the one hand, and all in- and out-of-plane deformations on the other hand.

2 Stacking sequence retrieval as an optimization problem

2.1 Laminated composite materials

Fiber-reinforced composite materials are heterogeneous materials consisting of fibers incorporated in a supportive matrix, which gives rise to an orthotropic material with distinct stiffness characteristics along the longitudinal and the orthogonal fiber-directions [78]. *Laminated composites* are formed by stacking multiple layers of this material, for which the anisotropic stiffness characteristics can be tailored to the unique strength requirements of a structure by adjusting the orientation of each ply (Figure 1 a).

For laminated composites, the mechanical behavior, to a first-order approximation, is typically characterized using a variation of Hooke's law [79–81]:

$$\begin{bmatrix} \vec{N} \\ \vec{M} \end{bmatrix} = \begin{bmatrix} \mathbf{A} & \mathbf{B} \\ \mathbf{B} & \mathbf{D} \end{bmatrix} \begin{bmatrix} \vec{\varepsilon}^0 \\ \vec{\kappa} \end{bmatrix}.$$

Here, the stress and moment resultants, \vec{N} and \vec{M} , represent the loadings within the structure. The deformations are characterized by $\vec{\varepsilon}^0$ (in-plane bending) and $\vec{\kappa}$ (out-of-plane bending). Figures 1 b and c illustrate the stress and moment resultants, along with the deformations, visually demonstrating their effects on the laminate. The **ABD**-matrix analogously functions as the stiffness tensor. Specifically, **A** and **D** define the in-plane and out-of-plane stiffness, respectively. A non-zero **B** indicates a coupling between them, meaning in-plane stresses can result from out-of-plane bending and vice versa. Both vectors \vec{N} and \vec{M} along with $\vec{\varepsilon}^0$ and $\vec{\kappa}$ consist of three components. Furthermore, matrices **A**, **B** and **D** are of dimensions 3×3 .

For a laminate defined by a specific stacking sequence, the **ABD**-matrix is completely determined by the thickness of the material, the angles of the individual plies, and the inherent properties of the selected composite material. Furthermore, these dependencies separate when introducing *lamination parameters*, which distill the complete ply-angle dependence of the **ABD**-matrix into exactly 12 real values v_l^A, v_l^B, v_l^D with $l = 1, 2, 3, 4$ [36, 37]. Denoting the laminate thickness with h , the **ABD**-matrix is determined by [41,

82]:

$$\begin{aligned}\mathbf{A} &= h(\mathbf{\Gamma}_0 + \mathbf{\Gamma}_1 v_1^A + \mathbf{\Gamma}_2 v_2^A + \mathbf{\Gamma}_3 v_3^A + \mathbf{\Gamma}_4 v_4^A), \\ \mathbf{B} &= \frac{h^2}{4}(\mathbf{\Gamma}_0 + \mathbf{\Gamma}_1 v_1^B + \mathbf{\Gamma}_2 v_2^B + \mathbf{\Gamma}_3 v_3^B + \mathbf{\Gamma}_4 v_4^B), \\ \mathbf{D} &= \frac{h^3}{12}(\mathbf{\Gamma}_0 + \mathbf{\Gamma}_1 v_1^D + \mathbf{\Gamma}_2 v_2^D + \mathbf{\Gamma}_3 v_3^D + \mathbf{\Gamma}_4 v_4^D),\end{aligned}\quad (1)$$

where the intrinsic material properties enter the equation in form of the matrices $\mathbf{\Gamma}_l$ with $l = 0, 1, 2, 3, 4$. For a stacking sequence comprising N plies of equal thickness and ply angles $\phi_1, \dots, \phi_N \in (-\pi/2, \pi/2]$, and the distance of ply n from the mid-plane captured in $z_n = -N/2 + n$, the lamination parameters read:

$$\begin{aligned}(v_1^A, v_2^A, v_3^A, v_4^A) &= \frac{1}{N} \sum_{n=1}^N (z_n - z_{n-1}) (\cos(2\phi_n), \sin(2\phi_n), \cos(4\phi_n), \sin(4\phi_n)), \\ (v_1^B, v_2^B, v_3^B, v_4^B) &= \frac{2}{N^2} \sum_{n=1}^N (z_n^2 - z_{n-1}^2) (\cos(2\phi_n), \sin(2\phi_n), \cos(4\phi_n), \sin(4\phi_n)), \\ (v_1^D, v_2^D, v_3^D, v_4^D) &= \frac{4}{N^3} \sum_{n=1}^N (z_n^3 - z_{n-1}^3) (\cos(2\phi_n), \sin(2\phi_n), \cos(4\phi_n), \sin(4\phi_n)).\end{aligned}\quad (2)$$

The matrices $\mathbf{\Gamma}_k$ are constructed with the Tsai-Pagano material invariants $U_1, \dots, U_5 \in \mathbb{R}$ [36]:

$$\begin{aligned}\mathbf{\Gamma}_0 &= \begin{bmatrix} U_1 & U_4 & 0 \\ U_4 & U_1 & 0 \\ 0 & 0 & U_5 \end{bmatrix}, \quad \mathbf{\Gamma}_1 = \begin{bmatrix} U_2 & 0 & 0 \\ 0 & -U_2 & 0 \\ 0 & 0 & 0 \end{bmatrix}, \quad \mathbf{\Gamma}_2 = \begin{bmatrix} 0 & 0 & U_2/2 \\ 0 & 0 & U_2/2 \\ U_2/2 & U_2/2 & 0 \end{bmatrix} \\ \mathbf{\Gamma}_3 &= \begin{bmatrix} U_3 & -U_3 & 0 \\ -U_3 & U_3 & 0 \\ 0 & 0 & -U_3 \end{bmatrix}, \quad \mathbf{\Gamma}_4 = \begin{bmatrix} 0 & 0 & U_3 \\ 0 & 0 & -U_3 \\ U_3 & -U_3 & 0 \end{bmatrix}.\end{aligned}$$

These material invariants depend only on the longitudinal, transverse, and shear moduli, as well as the Poisson's ratio of the composite.

In numerous applications, particularly in aerospace structural design, materials are required to be as lightweight as possible while simultaneously possessing the strength to withstand forces and stresses under a variety of expected loading conditions. A typical objective involves minimizing the thickness or, equivalently, the number of plies in composite materials. This minimization is constrained by the expected stress and moment resultants \vec{N} and \vec{M} , alongside predefined failure criteria expressed through inequalities involving stresses, deformations, or the **ABD**-matrix. The optimization process becomes highly complex due to the non-linear relationship between the laminate's structural behavior and the ply angles, which serve as design variables in the optimization and typically range from tens to hundreds in number [82]. To effectively navigate this complexity, a bi-level design strategy is commonly employed for laminated composite materials, involving two distinct phases of optimization [29–35]. The first phase optimizes for the laminate thickness h and the stiffness characteristics, represented by lamination parameters v_l^A , v_l^B and v_l^D , such that they meet predefined strength criteria. These design variables are typically assumed to be continuous, such that gradient descent methods can be employed effectively. The subsequent phase, termed *stacking sequence retrieval* (SSR), seeks a ply-angle sequence that approximates the lamination parameters derived from the first phase. The laminate thickness h is incorporated into the second phase as the total number of plies N in the laminate. In this work, we will focus on this second phase of stacking sequence retrieval.

Manufacturing constraints typically dictate the allowed ply-angle sequences in a laminate. Primary among these is the confinement of ply angles to a discrete set, with a common selection being $\{0^\circ, +45^\circ, 90^\circ, -45^\circ\}$. Alternatives can also be found, with divisions of the interval $(-\pi/2, \pi/2]$ at intervals of 22.5° or 15° . It is worth noting that fiber orientations, and consequently the lamination parameters, demonstrate a periodicity of 180° . Other prevalent manufacturing constraints include [38–41]:

- **Symmetric laminates:** The laminate exhibits symmetry about its midplane. Hence, plies n and $N - n + 1$ share the same ply angle, leading to null coupling lamination parameters v_k^B and stiffness matrix \mathbf{B} .

- **Disorientation constraint:** The angular difference between adjacent plies is limited, often to 45° .
- **Balanced laminates:** Except for ply-angles 0° or 90° , the number of plies with angles θ and $-\theta$ are equal. This has the effect, that v_2^A and v_4^A vanish.
- **Contiguity constraint:** The number of consecutive same-angle plies is limited, for instance to 5 plies with the same orientation.
- **10%-rule:** Specific ply angles must constitute a minimum of 10% of the laminate. This rule is frequently applied to angles of 0° , 90° and $\pm 45^\circ$.

For a laminate consisting of N plies and a set of d discrete angles, the solution space encompasses d^N potential configurations. This exponential explosion renders direct search or enumeration methods computationally prohibitive. Moreover, the imposition of manufacturing constraints further complicates the search landscape. Various strategies have been advanced to navigate this complex space [23, 25, 47, 83], however, the optimization of more complicated structures remains a formidable challenge.

Lately, there has been a spotlight on breakthroughs in quantum computing, a technology that might offer new tools to address this complexity [5, 7, 84–86]. However, one must map the presently-described problem to a representation amenable to quantum information-theoretic methods. We start with formulating stacking sequence retrieval as an integer-optimization problem.

2.2 Formulating stacking sequence retrieval as an integer-optimization problem

In general, it is advantageous for optimization algorithms to be presented with a version of the problem that abstracts away all but the essential information. For our purposes, this level of abstraction is necessary to adapt the problem for quantum computing architectures. In this section, we present our redefinition of the problem that forms the basis for our analysis in this work.

The discrete nature of the ply angles in laminated composites is well-suited to be represented in terms of integer design variables, a method commonly employed in various stacking sequence retrieval methods [35, 55, 87]. Accordingly, we define the d discrete angles $\Theta = \{\theta_1, \theta_2, \dots, \theta_d\}$, allowing each angle θ_s to be represented by its corresponding label $s \in \{1, \dots, d\}$, effectively using these labels as integer design variables. Consequently, we can identify the ply angle sequence $\vec{\theta} = (\theta_{s_1}, \theta_{s_2}, \dots, \theta_{s_N})$ with an ordered list of integers $\vec{s} = (s_1, s_2, \dots, s_N)$. Here we use θ instead of the ϕ from eq. (2), to convey that we now explicitly choose the ply angles from the discrete set Θ . In the following, we denote the set of all possible stacking sequences as $\mathcal{S} = \{1, \dots, d\}^N$, such that $\vec{s} \in \mathcal{S}$. Considering eq. (2), the lamination parameters can then be written in a common general form:

$$v_l^X(s_1, \dots, s_N) = \sum_{n=1}^N \alpha_n^X f_l(s_n), \quad (3)$$

where $X = A, B, D$ and $l = 1, 2, 3, 4$, and the functions $f_l : \{1, \dots, d\} \rightarrow [-1, 1]$ defined as:

$$\begin{aligned} f_1(s) &= \cos(2\theta_s), & f_2(s) &= \sin(2\theta_s), \\ f_3(s) &= \cos(4\theta_s), & f_4(s) &= \sin(4\theta_s). \end{aligned}$$

In this framework, a manufacturing constraint can be realized as a Boolean function $c : \mathcal{S} \rightarrow \{\text{True}, \text{False}\}$ on the lists of integers, where $c(\vec{s}) = \text{True}$ exactly when ply-angle sequence $\vec{\theta} = (\theta_{s_1}, \dots, \theta_{s_N})$ satisfies the constraint. The optimization towards target lamination parameters can then be written as an integer-optimization problem.

Stacking sequence retrieval problem (SSR): Given

- Positive integers $N, d \in \mathbb{N}$,
- The set of stacking sequences $\mathcal{S} = \{1, \dots, d\}^N$,
- Sets of weights $\{\alpha_n^X\}_n$ for $n = 1, \dots, N$ and $X = 1, \dots, N_\alpha$ for some $N_\alpha \in \mathbb{N}$,
- Functions $f_l : \{1, \dots, d\} \rightarrow \mathbb{R}$ for $l = 1, \dots, N_f$ for some $N_f \in \mathbb{N}$,
- A set of constraints $\mathcal{C} = \{c_k : \mathcal{S} \rightarrow \{\text{True}, \text{False}\}\}$ on the solution space, where k enumerates the constraints,
- Target values $\vec{\xi} \in \mathbb{R}^{N_\alpha N_f}$,

find a stacking sequence $\vec{s} = (s_1, \dots, s_N) \in \mathcal{S}$ with $c(\vec{s}) = \text{True}$ for all $c \in \mathcal{C}$ that minimizes the loss function:

$$H(s_1, \dots, s_N) = \sum_{X,l} \left(\sum_{n=1}^N \alpha_n^X f_l(s_n) - \xi_l^X \right)^2. \quad (4)$$

Note, that for the loss function, we use the mean-square-error (MSE) rather than the root-mean-square-error (RMSE), due to its natural implementation in the quantum context. Nevertheless, the RMSE can prove useful to evaluate the quality of solutions, as it represents the Euclidean distance of the solution to the target parameters in lamination parameter space. The defined integer-optimization problem is more general than the original stacking sequence retrieval problem, and most of the following discussion does not depend on explicit definitions of α_n^X , N_α , f_l and N_f . However, we will generally assume the previously defined case of $N_f = 4$, $X = A, B, D$ such that $N_\alpha = 3$, and α_n^X and f_l defined according to the lamination parameters in eq. (2).

3 A quantum formulation of the stacking sequence retrieval problem

In this section, we detail how we adapt the previously defined integer-optimization problem to be compatible with quantum computation. While our discussion will include clarifications of key quantum computing concepts, we recommend Nielsen and Chuang's textbook [7] as an introductory yet comprehensive resource for those seeking a deeper understanding of quantum computing.

A quantum computer is essentially a physical system that obeys the laws of quantum mechanics, and over which we have sufficient control, such that we can use it to perform calculations. In order to describe physical quantum systems, we generally use concepts from linear algebra. In particular, a state of a quantum system is represented by a vector in a Hilbert space. Other quantities, such as transformation of a state or measurable quantities, are defined as linear operators on this space. On a quantum computer, we control these transformations and measurements in order to perform calculations. Accordingly, we use the same linear algebra concepts to describe information content and operations on the quantum computer, which form the basis for quantum algorithms.

In this section, we apply these concepts to the SSR problem. First, we represent stacking sequences as quantum states. We then derive a linear operator, the Hamiltonian, that encapsulates the loss function of the SSR problem. Finally, we illustrate how the manufacturing constraints can be enforced by adding penalty terms to the Hamiltonian, such that we recover an effective unconstrained optimization problem. During this process, we will discuss implications of the Hamiltonian's specific form for the performance of quantum algorithms.

3.1 Translating stacking sequences to a quantum state space

A canonical procedure for translating a classical problem to a quantum formulation involves embedding the classical states – here represented as ordered lists of integers $\vec{s} \in \mathcal{S}$ with $\mathcal{S} = \{1, \dots, d\}^N$ – as basis vectors in a *complex-valued Hilbert space*. For each ply $n \in \{1, 2, \dots, N\}$, which can take on d different states corresponding to the available ply angles, we define a Hilbert space \mathcal{H}_n with $\dim(\mathcal{H}_n) = d$, where each ply angle $s \in \{1, \dots, d\}$ maps to a basis vector $|s\rangle$:

$$\mathcal{H}_n = \text{span}(\{|s\rangle\}_{s=1, \dots, d}).$$

Consistent with standard practice in quantum information science, we employ Dirac notation, wherein a vector is denoted with brackets $|\cdot\rangle$. The dual of the vector $|\psi\rangle$ is $\langle\psi|$, and the inner product between two vectors $|\psi\rangle$ and $|\phi\rangle$ is $\langle\phi|\psi\rangle$. The basis vectors are assumed to be orthogonal:

$$\langle s|t\rangle = \delta_{st},$$

where $s, t \in \{1, \dots, d\}$, and δ_{st} is the Kronecker delta. For the entire laminate, the individual ply Hilbert spaces are tensorially combined as:

$$\mathcal{H} = \mathcal{H}_1 \otimes \mathcal{H}_2 \otimes \dots \otimes \mathcal{H}_N,$$

yielding $\dim(\mathcal{H}) = d^N$. Stacking sequences $\vec{s} = (s_1, \dots, s_N) \in \mathcal{S}$ correspond to the orthonormal basis vectors of the composite space:

$$|\vec{s}\rangle = |s_1 s_2 \cdots s_N\rangle = |s_1\rangle \otimes |s_2\rangle \otimes \cdots |s_N\rangle \in \mathcal{H}.$$

We can now represent any linear combination of these basis states as:

$$|\psi\rangle = \sum_{\vec{t} \in \mathcal{S}} \psi_{\vec{t}} |\vec{t}\rangle$$

with specified coefficients $\psi_{\vec{t}} \in \mathbb{C}$. We usually do not have direct access to the complete information content of a state $|\psi\rangle \in \mathcal{H}$. Instead, a *measurement* of the state yields basis state $|\vec{s}\rangle$ with probability:

$$P_{\vec{s}}(\psi) = \langle \vec{s} | \psi \rangle = |\psi_{\vec{s}}|^2,$$

if the state is normalized, which we generally assume to be the case:

$$\langle \psi | \psi \rangle = \sum_{\vec{t} \in \mathcal{S}} |\psi_{\vec{t}}|^2 = 1.$$

3.2 Constructing the loss function Hamiltonian

While states are represented as vectors in a Hilbert space, other quantities are generally expressed through linear operators on the Hilbert space. We denote the space of Endomorphisms of a Hilbert space \mathcal{H} with:

$$\mathcal{L}(\mathcal{H}) = \left\{ \hat{A} : \mathcal{H} \rightarrow \mathcal{H} \mid \hat{A}(\alpha |\phi\rangle + \beta |\xi\rangle) = \alpha \hat{A} |\phi\rangle + \beta \hat{A} |\xi\rangle \quad \text{for } |\phi\rangle, |\xi\rangle \in \mathcal{H}, \alpha, \beta \in \mathbb{C} \right\}.$$

As it is common in quantum science, linear operators are marked with a hat symbol. Similar to how a state in the Hilbert space is decomposed in terms of a given basis, we frequently express a linear operator $\hat{A} \in \mathcal{L}(\mathcal{H})$ in terms of its matrix elements:

$$\hat{A} = \sum_{\vec{u}, \vec{t} \in \mathcal{S}} A_{\vec{u}, \vec{t}} |u\rangle \langle t|, \quad A_{\vec{u}, \vec{t}} = \langle \vec{u} | \hat{A} | \vec{t} \rangle.$$

Here, the dyadic product of basis vectors $|\vec{u}\rangle \langle \vec{t}|$ takes an analogous role to the basis vectors $|\vec{t}\rangle$ in a vector decomposition and can be defined via their action on an basis vector $|\vec{s}\rangle$:

$$(|\vec{u}\rangle \langle \vec{t}|) |\vec{s}\rangle = |\vec{u}\rangle \langle \vec{t} | \vec{s} \rangle = \delta_{t_1 s_1} \delta_{t_2 s_2} \cdots \delta_{t_N s_N} |\vec{t}\rangle.$$

We generally encounter linear operators for two different purposes: transformations of the state and observable quantities.

The operations on a quantum computer are transformations of its state. As described above, the components $\psi_{\vec{s}}$ of a state $|\psi\rangle$ encode the respective probabilities of obtaining basis state $|\vec{s}\rangle$ upon measurement of $|\psi\rangle$. Given that the sum of probabilities always equals 1, transformations of a quantum state, such as operations on a quantum computer, are thus required to preserve the norm $\langle \psi | \psi \rangle$. They are therefore unitary operators $\hat{U} \in \mathcal{L}(\mathcal{H})$:

$$\hat{U}^\dagger \hat{U} = \hat{I},$$

where $\hat{I} \in \mathcal{L}(\mathcal{H})$ is the identity on \mathcal{H} .

The second type of object that we describe with linear operators are observable quantities. In quantum mechanics, a measurement of an observable quantity only gives a predetermined, consistent result for specific states that together form an orthonormal basis of the Hilbert space. These states and according measurement values appear as eigenstates and eigenvalues of the linear operator $\hat{A} \in \mathcal{L}(\mathcal{H})$ that represents a given observable quantity. Since all eigenvalues are real and the eigenstates form an orthogonal basis, these linear operators are required to be Hermitian operators $\hat{A} = \hat{A}^\dagger$.

The definition of the SSR problem relies on functions $g : \mathcal{S} \rightarrow \mathbb{R}$ on the stacking sequences $\vec{s} \in \mathcal{S}$. These functions are therefore only determined for the basis states $|\vec{s}\rangle$, but so far not for a general state in \mathcal{H} . Reflecting the characteristics of observable quantities, a function $g(\vec{s})$ can be represented by a

Hermitian operator \hat{g} for which the basis vectors \vec{s} serve as its eigenvectors with eigenvalues corresponding to function evaluations:

$$\hat{g} |\vec{s}\rangle = g(\vec{s}) |\vec{s}\rangle.$$

Consequently, the operator \hat{g} has diagonal form when expressed via the basis vectors $|\vec{s}\rangle$:

$$\hat{g} = \sum_{\vec{t} \in \mathcal{S}} g(\vec{t}) |\vec{t}\rangle\langle\vec{t}|.$$

As a result, the operator aligns with expectation values derived from measurements of a state $|\psi\rangle = \sum_{\vec{s}} \psi_{\vec{s}} |\vec{s}\rangle$:

$$\langle \hat{g} \rangle_{\psi} = \langle \psi | \hat{g} | \psi \rangle = \sum_{\vec{t} \in \mathcal{S}} g(\vec{t}) |\psi_{\vec{t}}|^2.$$

Considering the loss function in eq. (4), the only components dependent on the ply angles are the functions f_l . We can construct the corresponding operator acting on individual ply Hilbert spaces \mathcal{H}_n as:

$$\hat{f}_l^{[n]} = \sum_{t=1}^d f_l(t) |t\rangle\langle t|_n.$$

The index n in $|t\rangle\langle t|_n$ signifies, that the operator acts on subsystem \mathcal{H}_n as $|t\rangle\langle t|$, and the identity on all other subsystems:

$$|t\rangle\langle t|_n |\vec{s}\rangle = \delta_{t,s_n} |\vec{s}\rangle.$$

Consequently, the resultant operator for loss function H , commonly denoted as the *Hamiltonian*, is:

$$\hat{H} = \sum_{X,l} \left(\sum_{n=1}^N \alpha_n^X \hat{f}_l^{[n]} - \xi_l^X \right)^2. \quad (5)$$

The notation assumes scalar terms, such as ξ_l^X here, to implicitly be multiplied by the identity operator, $\xi_l^X \hat{I}$, to obtain the correct dimension in a summation with other operators. By construction, the basis states $|\vec{s}\rangle \in \mathcal{S}$ are eigenvectors of the Hamiltonian \hat{H} with eigenvalues corresponding to the loss function value $H(\vec{s})$:

$$\hat{H} |\vec{s}\rangle = \sum_{X,l} \left(\sum_{n=1}^N \alpha_n^X f_l(s_n) - \xi_l^X \right)^2 |\vec{s}\rangle = H(\vec{s}) |\vec{s}\rangle,$$

since a basis state $|\vec{s}\rangle$ is also an eigenvector of $\hat{f}_l^{[n]}$ and consequently:

$$\left(\sum_{n=1}^N \alpha_n^X \hat{f}_l^{[n]} - \xi_l^X \right) |\vec{s}\rangle = \left(\sum_{n=1}^N \alpha_n^X f_l(s_n) - \xi_l^X \right) |\vec{s}\rangle.$$

The Hamiltonian has therefore a diagonal form:

$$\hat{H} = \sum_{\vec{t} \in \mathcal{S}} H(\vec{t}) |\vec{t}\rangle\langle\vec{t}|.$$

Hence, the state minimizing the loss function aligns with the Hamiltonian's eigenstate possessing the lowest eigenvalue, known as the *ground state*. This approach mirrors seeking the lowest-energy state of a physical quantum system, wherein the Hamiltonian is the energy operator.

Due to the description of quantum systems in terms of Hilbert spaces, vectors and linear operators, defining homomorphisms between distinct Hilbert spaces enables the formal transformation of one quantum system into another. Particularly, since quantum computers are quantum systems, the vectors and unitary and hermitian operators can be translated into corresponding quantum states, operations and measurements on a quantum computer [88–91]. Therefore, a quantum system can efficiently be represented on a quantum computer with an appropriately sized Hilbert space, which makes quantum computing a prime candidate for determining the properties of quantum systems [8, 15, 61, 65]. Algorithms proposed for finding the ground state of a quantum system's Hamiltonian encompass variational quantum algorithms (VQA) [66–69], quantum annealing [62, 70, 71, 92–94], and quantum phase estimation (QPE) [63, 64].

To gain deeper insight into the loss function Hamiltonian in eq. (5), we decompose it into local operators acting on individual subsystems \mathcal{H}_n . For a Hamiltonian representing a physical systems, a product of local operators of two or more distinct subsystems describes an interaction between these subsystems. As we outline further below, the exact form of these interaction terms has a major impact on the applicability and efficiency of quantum algorithms and classical numerical approaches. To retrieve the loss function Hamiltonian in terms of local operators, we incorporate the target values ξ_l^X directly into the terms of the summation indexed by the plies n . Given that for lamination parameters, the weights α_n^X collectively sum to 1:

$$\sum_{n=1}^N |\alpha_n^X| = 1,$$

we can achieve this naturally, by defining local operators on the subsystems $\mathcal{H}^{[n]}$ as:

$$\hat{H}_{X,l}^{[n]} = \alpha_n^X \left(\hat{f}_l^{[n]} - \text{sign}(\alpha_n^X) \xi_l^X \right)$$

allowing the Hamiltonian to be expressed as:

$$\hat{H} = \sum_{X,l} \left(\sum_{n=1}^N \hat{H}_{X,l}^{[n]} \right)^2. \quad (6)$$

It is worth noting that for the A - and D -parameters, all the weights are positive, i.e., $\alpha_n^A, \alpha_n^D > 0$, rendering the sign function redundant.

Examining the expanded Hamiltonian in eq. (6):

$$\hat{H} = \sum_{n,m=1}^N \sum_{X,l} \hat{H}_{X,l}^{[n]} \hat{H}_{X,l}^{[m]}, \quad (7)$$

reveals that the Hamiltonian incorporates interactions between each subsystem pair, but no higher-order terms. As we discuss further down, the fundamental units of most quantum computers are so-called qubits, and contemporary quantum computers primarily utilize operations involving two qubits, also known as two-qubit gates. Generally, higher-order gates need to be decomposed into two-qubit gates, which increases the runtime of an algorithm. In algorithms, that rely on implementing the interactions as operations on the qubits, having only quadratic terms in the loss function Hamiltonian omits the need for these decompositions. Nevertheless, having an interaction term for each subsystem pair is unusual for physical systems, where subsystems typically exhibit interactions primarily with their nearest neighbors.

Some architectures for quantum computers, such as those based on superconducting qubits [6, 95], rely on this local connectivity. As a result, implementing a Hamiltonian with a more complex entanglement structure can lead to an increase in the number of operations required and potentially expand the number of qubits needed. Quantum annealers, for instance, are particularly sensitive to these requirements due to their specialized architecture [62, 70, 71, 92–94]. On the other hand, certain quantum computing platforms, like specific ion trap systems [96–98], inherently support a longer-range connectivity, which aligns better with the Hamiltonian’s implied interaction complexity. Therefore, the successful implementation of such a Hamiltonian in quantum algorithms greatly depends on the careful consideration of the underlying quantum computing architecture. We leave the treatment of our formulation for specific quantum architectures to future work.

In the suggested quantum representation, subsystems have a dimension of $\dim(\mathcal{H}_n) = d$, typically ranging between 4 and 12. In principle, a quantum computer could consist of units with an equivalent dimension, commonly termed a *quantum digit* or *qudit*. However, present quantum hardware primarily employs two-dimensional subsystems known as *quantum bits* or *qubits*, characterized by two basis states $|0\rangle$ and $|1\rangle$. Analogous to representing integers with multiple bits in classical systems, several qubits can collectively represent a quantum digit. Depending on the chosen algorithm, different approaches can be utilized. Some, such as a binary encoding, prioritize qubit efficiency, others, including a one-hot encoding, preserve the quadratic structure of the Hamiltonian [99, 100].

3.3 Incorporating manufacturing constraints

In addition to optimizing for the target lamination parameters, it is essential to ensure that the stacking sequences adhere to manufacturing constraints, like the ones listed in section 2. In this section, we examine

how these constraints, generalized to larger classes of constraints, can be enforced.

Some constraints can be directly incorporated into the representation of the stacking sequences. For instance, to enforce symmetry around the midplane in a laminate, $s_n = s_{N-n+1}$, it suffices to model half of the stack and then implicitly mirror this to the other half. Due to the symmetry of the weights, the A and D lamination parameters in eq. (2) can be adapted to this case, by only summing the upper half $n = N/2 + 1, \dots, N$ of the stack and doubling the result. For a more convenient expression, we can reassign the ply indices n to start at the midplane by substituting $n \rightarrow n - N/2$, such that $z_n = n$. We also redefine the ply number N to just count half of the stack $N/2 \rightarrow N$. The reformulated lamination parameters only differ from eq. (2) by the definition of z_n and the factor 4 preceding the summation in the D -parameters:

$$\begin{aligned} (v_1^A, v_2^A, v_3^A, v_4^A) &= \frac{1}{N} \sum_{n=1}^N (z_n - z_{n-1}) (\cos(2\theta_n), \sin(2\theta_n), \cos(4\theta_n), \sin(4\theta_n)) \\ (v_1^D, v_2^D, v_3^D, v_4^D) &= \frac{1}{N^3} \sum_{k=1}^N (z_n^3 - z_{n-1}^3) (\cos(2\theta_n), \sin(2\theta_n), \cos(4\theta_n), \sin(4\theta_n)) \\ z_n &= n \end{aligned} \quad (8)$$

As before, the weights

$$\alpha_n^A = \frac{1}{N}, \quad \alpha_n^D = \frac{n^3 - (n-1)^3}{N^3}$$

sum to 1. The B -parameters vanish for symmetric laminates and can thus be neglected.

Other constraints might be enforced with methods specific to the quantum algorithm at hand. An algorithm-independent way of enforcing a constraint $c : \mathcal{S} \rightarrow \{\text{True}, \text{False}\}$ can be achieved by incorporating a penalty function $H_c : \mathcal{S} \rightarrow \mathbb{R}_{\geq 0}$ into the loss function:

$$H_{\text{total}}(\vec{s}) = H(\vec{s}) + H_c(\vec{s}),$$

where $H_c(\vec{s}) > 0$ if the constraint is violated for stacking sequence \vec{s} , $c(\vec{s}) = \text{False}$, and $H_{\text{penalty}}(\vec{s}) = 0$ for valid states, $c(\vec{s}) = \text{True}$. This effectively turns the constraint optimization problem with loss function H into an unconstrained optimization problem with loss function H_{total} [101–103].

As with the loss function H , the penalty function H_c is also transformed into a linear operator \hat{H}_c for its quantum representation. Consequently, the total Hamiltonian takes the form

$$\hat{H}_{\text{total}} = \hat{H} + \hat{H}_c.$$

As discussed for the Hamiltonian \hat{H} , the interactions between subsystems in \hat{H}_c significantly influence the performance of various quantum algorithms. In the following, we explore possible penalty terms for the remaining manufacturing constraints apart from the symmetry constraint in section 2. For this purpose, we examine general categories of constraints that encompass the listed constraints.

3.3.1 The disorientation constraint as nearest-neighbor coupling

The simplest constraint listed in section 2 is the disorientation constraint, which limits the ply angle difference between neighboring plies. In general, a constraint with nearest neighbor coupling can be enforced with a penalty function $\eta : \{1, \dots, d\}^2 \rightarrow \mathbb{R}_{\geq 0}$ on each pair of neighboring subsystems n and $n+1$:

$$\eta(s_n, s_{n+1}) = \begin{cases} \gamma, & \text{if } (s_n, s_{n+1}) \text{ violates the constraint,} \\ 0, & \text{else,} \end{cases}$$

where the adjustable parameter $\gamma > 0$ is the added penalty for a single constraint violation. The function η is used to define an operator:

$$\hat{H}_{\text{nn}}^{[n, n+1]} = \sum_{t, t'=1}^d \eta(t, t') |tt'\rangle \langle tt'|_{n, n+1}.$$

As before, the indices of $|tt'\rangle\langle tt'|_{n,n+1}$ signify the local action of the operator on subsystems \mathcal{H}_n and \mathcal{H}_{n+1} . Subsequently, these operators are summed over all nearest-neighbor pairs to yield the total penalty:

$$\hat{H}_{\text{nn}} = \sum_{n=1}^{N-1} \hat{H}_{\text{nn}}^{[n,n+1]}. \quad (9)$$

The penalty operator exhibits strong parallels with quantum systems that feature nearest-neighbor coupling, such as spin lattice systems, and extensive research has been conducted on these systems [6, 70, 89, 93, 97, 104–108].

3.3.2 The contiguity constraint as k -local coupling

The contiguity constraint restricts the number of consecutive same-angle plies to be equal or less than some small integer N_{same} . A suitable penalty function evaluates $N_{\text{same}} + 1$ neighboring plies, and adds a penalty, if all plies have the same angle. The contiguity constraint is therefore a special case of a k -local constraint with $k = N_{\text{same}} + 1$, that encompasses interactions in a neighborhood of k subsystems in a linear chain. The treatment of nearest-neighbour interactions above can be extended to accommodate this case, by defining:

$$\eta(s_n, s_{n+1}, \dots, s_{n+k-1}) = \begin{cases} \gamma, & \text{if } (s_n, s_{n+1}, \dots, s_{n+k-1}) \text{ violates the constraint,} \\ 0, & \text{else,} \end{cases}$$

on k consecutive subsystems. As before, the parameter γ controls the magnitude of the added penalty. The corresponding k -local operator is given by:

$$\hat{H}_{k\text{-local}}^{[n,\dots,n+k-1]} = \sum_{t_1,\dots,t_k=1}^d \eta(t_1, \dots, t_k) |t_1 \dots t_k\rangle\langle t_1 \dots t_k|_{n,\dots,n+k-1}.$$

The total penalty takes the form:

$$\hat{H}_{k\text{-local}} = \sum_{n=1}^{N-k+1} \hat{H}_{k\text{-local}}^{[n,\dots,n+k-1]}.$$

Some algorithms, such as the quantum approximate optimization algorithm (QAOA) [67] or quantum phase estimation (QPE) [63, 64] require the implementation of interactions as operations. These higher-order terms typically require decomposition into two-qubit operations, leading to a significant increase in the total number of operations. Similarly, quantum annealers, which inherently support only second-order interactions, necessitate the transformation of higher-order terms into quadratic forms [62, 70, 71, 92–94]. This often involves the introduction of auxiliary qubits as additional variables [109–112]. Nonetheless, with advancements in quantum technology, future devices could be capable of managing these heightened operational demands, especially if k remains within a manageable range.

3.3.3 Balanced laminates and ensuring the same ply count for two distinct states

The constraint for balanced laminates requires that the ply angle sequence contains an equal number of plies with angle $+\theta$ and angle $-\theta$, provided θ is neither 0° nor 90° . This represents a special case of constraints where two states, denoted with t and t' , appear an equal number of times in the stacking sequence:

$$\sum_{n=1}^N \delta_{s_n, t} = \sum_{n=1}^N \delta_{s_n, t'}.$$

To implement such a penalty function, we can take the squared difference, similar to the loss function of the lamination parameters in eq. (4):

$$H_{\text{balanced}}(\vec{s}) = \gamma \left(\sum_{n=1}^N \delta_{s_n, t} - \sum_{n=1}^N \delta_{s_n, t'} \right)^2 = \gamma \left(\sum_{n=1}^N (\delta_{s_n, t} - \delta_{s_n, t'}) \right)^2$$

As before, the magnitude of the penalty can be adjusted with the parameter $\gamma \in \mathbb{R}_{>0}$. The corresponding operator is then:

$$\hat{H}_{\text{balanced}} = \gamma \left(\sum_{n=1}^N (|t\rangle\langle t|_n - |t'\rangle\langle t'|_n) \right)^2,$$

where $|t\rangle\langle t|_n - |t'\rangle\langle t'|_n$ is a local operator acting on subsystem n . This leads to a structure analogous to the Hamiltonian in eq. (7) for the lamination parameters, featuring interactions between each pair of subsystems. Consequently, the earlier considerations regarding quantum algorithms are also relevant here.

3.3.4 The 10%-rule and constraints on the ply count for a given state

The last manufacturing constraint listed in section 2 is the 10%-rule, which necessitates that certain ply angles, typically $0^\circ, 90^\circ$ or $\pm 45^\circ$, make up at least 10% of the plies. This constitutes a special case of constraints that, for some state t , require at least N_t plies to be in state t . A suitable penalty function can be defined as:

$$H_{\text{10%-rule}}(\vec{s}) = \begin{cases} 0, & \text{if } \sum_{n=1}^N \delta_{s_n, t} \geq N_t, \\ p(N_t - \sum_{n=1}^N \delta_{s_n, t}), & \text{else,} \end{cases} \quad (10)$$

where the function $p(x)$ characterizes the behavior for constraint violations. Examples include constant, $p(x) = \gamma$, linear $p(x) = \gamma x$ or power-law $p(x) = \gamma x^\alpha$ behavior for some $\alpha, \gamma > 0$. The according operator is defined as:

$$\hat{H}_{\text{10%-rule}} = \sum_{\vec{t} \in \mathcal{S}} H_{\text{10%-rule}}(\vec{t}) |\vec{t}\rangle\langle\vec{t}|.$$

As before, decomposing the operator into local operators provides insight into dependencies between individual subsystems. As we show in the appendix A.1, any penalty operator suitable for the 10%-rule contains terms of order $N - N_t + 1$ or larger. For the 10%-rule specifically, $N_t = 0.1N$, the operator contains terms that include roughly 90% of all subsystems. These high-order interactions present a notable challenge for many algorithms. Further investigation is vital to determine if and how these interactions can be efficiently managed in quantum algorithms.

4 Mapping the quantum problem to a tensor network representation

In the previous section 3, we represented stacking sequences in a quantum state space and developed a Hamiltonian that captures the loss function in eq. (4) of the integer-optimization problem defined in section 2.2, such that the ground state of this Hamiltonian constitutes the optimal solution of the problem. As mentioned before, several classical and quantum algorithms have been developed to solve these types of problems. To demonstrate the validity of our approach and get a first insight into the performance of ground-state solvers applied to our approach in general, our next step was the selection of one of these algorithms for detailed investigation.

Current quantum devices are still limited in the number of qubits. In addition, these qubits are susceptible to errors that accumulate throughout the algorithm's runtime and therefore hinder the execution of quantum algorithms that require a large number of operations [86, 113]. This poses a significant constraint on the ply count N of a laminate, for which we can effectively perform quantum algorithms on current devices.

Classical simulations offer an alternative, however the number of components $\psi_{\vec{s}}$ of a state vector $|\psi\rangle$:

$$|\psi\rangle = \sum_{\vec{s} \in \mathcal{S}} \psi_{\vec{s}} |\vec{s}\rangle,$$

which equals the dimension of the Hilbert space, grows exponentially in the number of subsystems $\dim(\mathcal{H}) = d^N$. This renders the direct simulation of quantum algorithms on classical hardware infeasible for systems with a significant ply count N . Despite these challenges, in the field of computational quantum physics, methods have been developed to find the ground-state of large quantum systems. A widespread

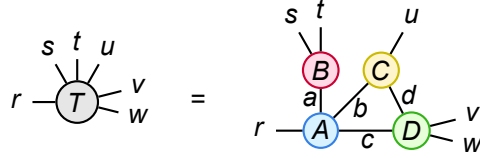


Figure 2: Example of a small tensor network $T_{rstuvw} = \sum_{abcd} A_{rabc} B_{sat} C_{bud} D_{cdvw}$ in tensor diagram notation [115]. Tensors are drawn as shapes, while tensor contractions are drawn as links between the tensors.

approach is the use of tensor network methods, of which the Density Matrix Renormalization Group (DMRG) algorithm is predominantly employed for one-dimensional quantum systems, similar to our quantum formulation of the SSR problem [72–77, 114]. Consequently, we selected the DMRG algorithm for our numerical calculations in order to demonstrate the application of ground-state optimization to our approach. While our focus so far has been on quantum computing, we note that this approach constitutes a novel quantum-inspired approach to SSR.

In the following section, we give a brief introduction of the relevant concepts, namely tensor networks, matrix product states and operators, and the DMRG algorithm. Subsequently, we demonstrate how the Hamiltonian in eq. (6) can be brought into matrix product operator (MPO) form, the tensor network structure necessary for the DMRG algorithm. Similarly, we present the penalty operator for the disorientation constraint in section 3.3.1 in MPO form, which we also include in our numerical simulations. For the remaining penalty operators in section 3.3, MPO forms are presented in the appendix (appendix A.3).

4.1 A brief introduction into relevant tensor network concepts

As mentioned above, the exponential dependency of the number of components ψ_s of a state vector $|\psi\rangle \in \mathcal{H}$ on the number of subsystems N , presents a notable difficulty for any classical simulation of large quantum system. Despite these obstacles, *tensor networks* serve as a powerful tool for representing a wide range of states in quantum many-body systems on classical hardware, effectively addressing the challenges of dimensionality [116–121]. They achieve this by representing a higher-order tensor, such as the components $\psi_{s_1 s_2 \dots s_N}$, as a collection of low-order tensors (for an example, see Figure 2), which mitigates the need of storing d^N components. Further below, we will illustrate this storage efficiency in the context of the matrix product state, the specific tensor network structure employed in our demonstration. A significant obstacle in using tensor networks is the potential exponential growth of an intermediate tensor during network contraction, making certain tensor contractions infeasible. By selectively representing states using tensor networks that can be efficiently contracted, a wide range of states can be effectively simulated. In the terminology of quantum information theory, we say that we constrain a property of the state known as *entanglement entropy*, as opposed to considering the system's overall size [107, 122–125]. This property quantifies the degree of correlations between distinct parts of the system and has an impact on whether a given state can efficiently be contracted on classical hardware. While entanglement entropy is a fundamental concept in the context of tensor networks, we will omit a detailed discussion of this term to maintain clarity and focus. Our demonstration employs the *density matrix renormalization group (DMRG) algorithm*, a potent tensor network algorithm for deducing the ground state of one-dimensional quantum many-body systems [72–77, 114]. The algorithm encodes state components using a one-dimensional chain of site tensors $\psi^{[n]}$ (Figure 3 a):

$$\psi_{s_1 s_2 \dots s_N} = \sum_{k_1 k_2 \dots k_{N-1}} \psi_{s_1, k_1}^{[1]} \psi_{s_2, k_1 k_2}^{[2]} \psi_{s_3, k_2 k_3}^{[3]} \dots \psi_{s_N, k_{N-1}}^{[N]},$$

yielding the *matrix product state (MPS)* structure [76, 77, 126–130]. The so-called bond indices k_n connect the individual local tensors through contraction, with the bond dimension representing the number of possible values each bond index can take. By denoting the maximum bond dimension as b , we find that each site tensor contains $O(db^2)$ elements. This results in the total number of elements scaling as $O(Ndb^2)$. Such scaling demonstrates how MPS can efficiently represent a variety of states while bypassing the need to store d^N floating-point values. Due to its linear structure, dividing the MPS into two parts only requires cutting a single bond. Hence, while evaluating the tensor contractions, for example to calculate scalar values like inner products and expectation values, the dimensions of the intermediate tensor stays

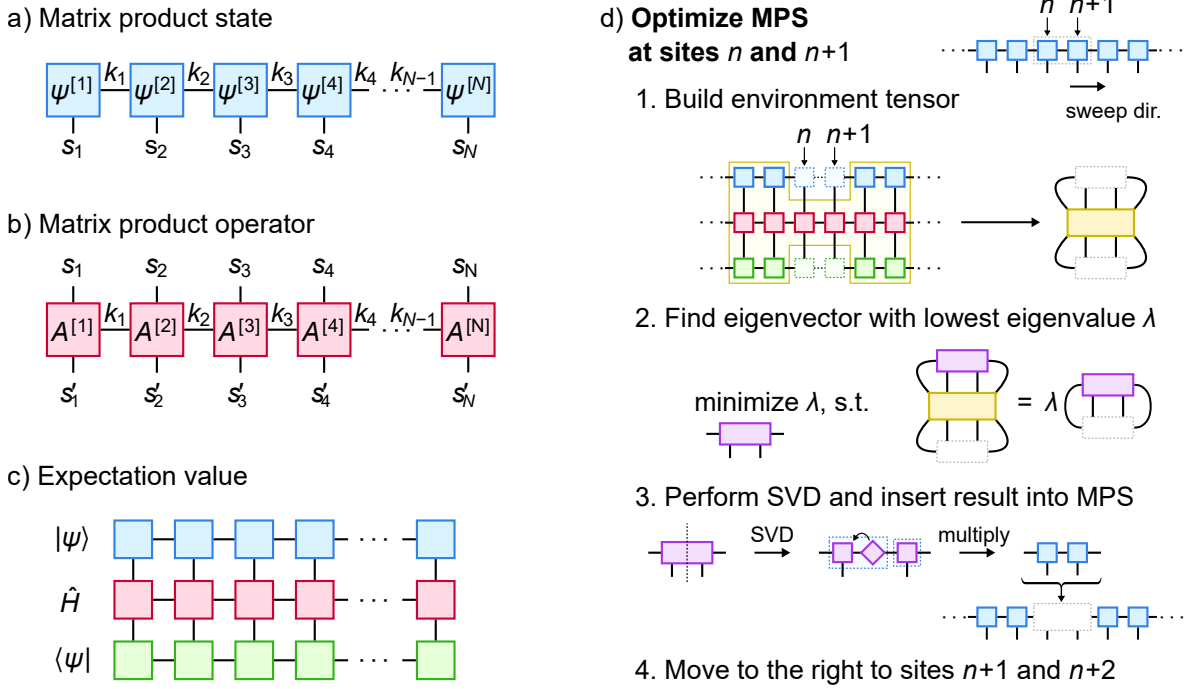


Figure 3: Relevant tensor network concepts in tensor diagram notation. a) A matrix product state (MPS) representing the components $\psi_{s_1 \dots s_N} = \langle \vec{s} | \psi \rangle$ of a state $|\psi\rangle$. b) A matrix product operator (MPO) representing the matrix elements $A_{s_1 \dots s_N, s'_1 \dots s'_N} = \langle \vec{s} | \hat{A} | \vec{s}' \rangle$ of an operator \hat{A} . c) The tensor network for the expectation value $\langle \psi | \hat{H} | \psi \rangle$ of Hamiltonian \hat{H} . d) Procedure for optimizing the MPS at positions n and $n + 1$. The multiplication of the singular matrix in step 3 to the left corresponds to sweeping to the right.

constant. The representation of a given state as an MPS is not unique, and there exists some flexibility in choosing the tensor elements with a focus on a particular application. This so-called gauge freedom plays a crucial role in the DMRG algorithm, as its optimization steps depend on the MPS being in particular gauges – particular forms of the MPS – which will be relevant in section 5.

The DMRG algorithm also requires operators in the *matrix product operators (MPO)* form [76, 77, 131, 132]. Analogous to vectors represented by components, an operator \hat{A} can be described in terms of its matrix element terms:

$$\hat{A} = \sum_{\vec{s}, \vec{s}'} A_{\vec{s}, \vec{s}'} | \vec{s} \rangle \langle \vec{s}' |, \quad A_{\vec{s}, \vec{s}'} = \langle \vec{s} | \hat{A} | \vec{s}' \rangle.$$

An MPO, similar to an MPS, consists of a tensor chain, but with doubled indices (Figure 3 b):

$$A_{s_1 s_2 \dots s_N, s'_1 s'_2 \dots s'_N} = \sum_{k_1 k_2 \dots k_{N-1}} A_{s_1 s'_1, k_1}^{[1]} A_{s_2 s'_2, k_1 k_2}^{[2]} A_{s_3 s'_3, k_2 k_3}^{[N]} \dots A_{s_N s'_N, k_{N-1}}^{[N]}.$$

The DMRG algorithm identifies the ground state of a Hamiltonian \hat{H} by sequentially optimizing the local tensors $\psi^{[n]}$ with respect to the expectation value $\langle \psi | \hat{H} | \psi \rangle$. This expectation value is constructed by contracting the open indices of the MPS and MPO representations of $|\psi\rangle$, \hat{H} , and $\langle \psi|$, as illustrated in Figure 3 c.

To facilitate a clearer understanding of the numerical results in section 5, we present a high-level overview of the DMRG algorithm’s mechanics. For in-depth details, we refer to the relevant literature [76, 77, 128]. Typically, the mentioned local optimizations involve pairs of adjacent tensors at positions n and $n + 1$. An illustration of this local optimization in tensor network notation is given in Figure 3 d. The local optimization starts with constructing an environment tensor around positions n and $n + 1$ from the tensor network representing the expectation value of the Hamiltonian $\langle \psi | \hat{H} | \psi \rangle$. Next, the eigenvector of the environment tensor with the lowest eigenvalue is found, which locally minimized the Hamiltonian expectation value. This is typically done with an iterative solver, such as the Lanczos algorithm [133, 134]. A singular value decomposition (SVD) on the resulting eigenvector creates three tensors: two new

local tensors at the respective positions n and $n + 1$, which are separated by a diagonal matrix containing the singular values. This diagonal matrix is then multiplied to one of the other two tensors, to retrieve the two optimized local tensors to be inserted in the MPS.

It should be noted, that for the local optimization to be an eigenvalue problem of the environment tensor, the MPS has to be in a certain gauge, which is often referred to as canonical form. However, an MPS can always be transformed into the required gauge using a prescribed sequence of singular value decompositions and tensor multiplications on the local tensors of the MPS. This also affects to which tensor the singular matrix must be multiplied. If the singular is multiplied to the tensor at site n , then the MPS is in canonical form for performing the next optimization one site over on sites $n + 1$ and $n + 2$. Conversely, multiplying the singular matrix to the tensor at site $n + 1$ prepares the MPS for a subsequent optimization on sites $n - 1$ and n . Consequently in standard DMRG implementations, local optimizations are executed sequentially, starting from one end of the MPS and progressing towards the other.

The complete optimization process involves multiple sweeps across the entire MPS. When alternating sweep directions, the next sweep can commence immediately from the endpoint of the previous sweep. For consistently sweeping in same the direction, additional operations on the MPS are required between sweeps to maintain the necessary gauge.

Without further measures, this optimization procedure can lead to exponential growth in the bond dimensions of the MPS. However, the diagonal matrix obtained during SVD, containing the singular values, provides a means to regulate the bond dimension. This is achieved by discarding the least significant singular values, thereby reducing the bond dimension. Consequently, a maximum bond dimension is can effectively be enforced.

In our numerical experiments, as detailed in section 5, we incorporate a disorientation constraint. The subsequent sections outline how the Hamiltonian, expressed in eq. (6), along with the penalty for nearest-neighbor constraints like the disorientation constraint (eq. (9)), can be formulated in MPO form. Representations for the other constraints discussed in section 3.3 are provided in the appendix (appendix A.3) for reference.

4.2 An MPO representation of the loss function Hamiltonian

In this section, we derive an MPO representation for the loss function Hamiltonian in eq. (6) from section 4.2. As we discuss further below, a summation of matrix product operators can be easily implemented in MPO form. Therefore, our initial focus is on a single term $\hat{H}_{X,l}$ corresponding to lamination parameter v_l^X :

$$\hat{H} = \sum_{X,l} \hat{H}_{X,l}, \quad \hat{H}_{X,l} = \left(\sum_{n=1}^N \hat{H}_{X,l}^{[n]} \right)^2.$$

The local operators $\hat{H}_{X,l}^{[n]}$ can be expressed in terms of their eigenvalues:

$$\hat{H}_{X,l}^{[n]} = \sum_{t=1}^d h_t^{[n]} |t\rangle\langle t|_n,$$

where $h_t^{[n]}$ denotes the t -th eigenvalue of $\hat{H}_{X,l}^{[n]}$, associated with the basis state $|t\rangle$ of \mathcal{H}_n , and is defined as:

$$h_t^{[n]} = \alpha_n^X (f_l(t) - \text{sign}(\alpha_n^X) \xi_l^X).$$

To construct an MPO representation of $\hat{H}_{X,l}$, it is necessary to decompose its matrix elements as discussed in the previous section, which are given by:

$$\begin{aligned} \langle \vec{s}' | \hat{H}_{X,l} | \vec{s} \rangle &= \langle \vec{s}' | \left(\sum_{n=1}^N \hat{H}_{X,l}^{[n]} \right)^2 | \vec{s} \rangle \\ &= \langle \vec{s}' | \vec{s} \rangle \left(\sum_{n=1}^N h_{s_n}^{[n]} \right)^2 \\ &= \delta_{s'_1, s_1} \cdots \delta_{s'_N, s_N} h_{\vec{s}}. \end{aligned} \tag{11}$$

Here we utilized that $|\vec{s}\rangle$ is an eigenvector:

$$\sum_{n=1}^N \hat{H}_{X,l}^{[n]} |\vec{s}\rangle = \sum_{n=1}^N h_{s_n}^{[n]} |\vec{s}\rangle,$$

and denote the eigenvalue of $\hat{H}_{X,l}$ for basis vector $|\vec{s}\rangle$ as:

$$h_{\vec{s}} = h_{s_1 \dots s_N} = \left(\sum_{n=1}^N h_{s_n}^{[n]} \right)^2, \quad \hat{H}_{X,l} |\vec{s}\rangle = h_{\vec{s}} |\vec{s}\rangle.$$

If the tensor $h_{s_1 s_2 \dots s_N}$ is expressed in MPS form:

$$h_{s_1 s_2 \dots s_N} = W_{s_1}^{[1]} W_{s_2}^{[2]} \dots W_{s_N}^{[N]},$$

the Kronecker delta $\delta_{s_n s'_n}$ can be multiplied to the matrices $W_{s_n}^{[n]}$:

$$W_{s_n s'_n}^{[n]} = W_{s_n}^{[n]} \delta_{s_n s'_n}$$

to obtain the matrix elements in eq. (11) of $\hat{H}_{X,l}$ in MPO form:

$$\langle \vec{s}' | \hat{H}_{X,l} | \vec{s} \rangle = W_{s_1 s'_1}^{[1]} W_{s_2 s'_2}^{[2]} \dots W_{s_N s'_N}^{[N]}. \quad (12)$$

Our approach to decompose $h_{\vec{s}}$ employs a matrix, that under repeated multiplications will produce $h_{\vec{s}}$ as the top-right element. For this purpose, we define the matrix:

$$M(x) = \begin{bmatrix} 1 & \sqrt{2}x & x^2 \\ 0 & 1 & \sqrt{2}x \\ 0 & 0 & 1 \end{bmatrix},$$

which multiplies as:

$$M(x)M(y) = M(x+y).$$

By induction, if we multiply N of these matrices with the eigenvalues $h_{s_n}^{[n]}$, we will find $h_{\vec{s}}$ as the top-right element of the resulting matrix:

$$\prod_{n=1}^N M(h_{s_n}^{[n]}) = M \left(\sum_n h_{s_n}^{[n]} \right) = \begin{bmatrix} 1 & \sqrt{2} \left(\sum_n h_{s_n}^{[n]} \right) & \left(\sum_n h_{s_n}^{[n]} \right)^2 \\ 0 & 1 & \sqrt{2} \left(\sum_n h_{s_n}^{[n]} \right) \\ 0 & 0 & 1 \end{bmatrix}.$$

An MPO representation of $\hat{H}_{X,l}$ as in eq. (12) can thus be acquired by decomposing it into matrices:

$$W_{s_n s'_n}^{[n]} = \delta_{s_n s'_n} M(h_{s_n}^{[n]})$$

for $1 < n < N$, and selecting the first row and third column at the first and last matrix respectively to obtain $\left(\sum_n h_{s_n}^{[n]} \right)^2$:

$$W_{s_1 s'_1}^{[1]} = [1 \ 0 \ 0] \delta_{s_1 s'_1} M(h_{s_1}^{[1]}),$$

$$W_{s_N s'_N}^{[N]} = \delta_{s_N s'_N} M(h_{s_N}^{[N]}) \begin{bmatrix} 0 \\ 0 \\ 1 \end{bmatrix}.$$

The total loss function Hamiltonian in eq. (6) is the sum of $\hat{H}_{X,l}$ for all lamination parameters $X = A, B, D$ and $l = 1, 2, 3, 4$, where $X = B$ can be excluded for symmetric laminates. The sum of matrix product operators (MPOs) can in principle be obtained by taking the direct product of the matrices $W_{s_n s'_n}^{[n]}$ for each n , effectively stacking them into block-diagonal matrices. However, due to the linearity of the expectation value $\langle \psi | \hat{H} | \psi \rangle$, DMRG is able to efficiently loop over the individual terms in the summation by calculating an environment tensor for each term individually and then adding these tensors element-wise to obtain the total environment tensor.

4.3 An MPO representation of nearest-neighbor constraints

As discussed in section 3.3, we can implement nearest-neighbor constraints as penalty functions, which can be expressed as operators and added to the Hamiltonian. The sum of the operators in eq. (9) effectively counts the constraint violations. There, we defined the added penalty for one constraint violation to be

$$\eta(s_n, s_{n+1}) = \begin{cases} \gamma, & \text{if } (s_n, s_{n+1}) \text{ violates constraint,} \\ 0, & \text{else,} \end{cases}$$

where $\gamma > 0$ is the penalty for a single constraint violation. Similar to other terms in the Hamiltonian, the penalty function needs to be represented as a matrix product operator (MPO). As before, we construct a matrix that calculates the desired result, which is the count of constraint violations, in the top-right corner. For this purpose, we represent the function $\eta(s_n, s_{n+1})$ as the dot product of two vectors $\vec{p}(s_n)$ and $\vec{q}(s_{n+1})$, both of dimension d :

$$\eta(s_n, s_{n+1}) = \vec{p}(s_n) \cdot \vec{q}(s_{n+1}) = \sum_{k=1}^d p_k(s_n) q_k(s_{n+1}).$$

We achieve this by using $\vec{p}(s_n)$ as an indicator for the state s_n , and $\vec{q}(s_{n+1})$ to indicate which neighboring state s_n leads to a constraint violation:

$$p_k(s_n) = \delta_{k, s_n}, \quad q_k(s_{n+1}) = \eta(k, s_{n+1}). \quad (13)$$

If we define a matrix $M(s)$ based on \vec{p} and \vec{q} as:

$$M(s) = \begin{bmatrix} 1 & p_1(s) & \cdots & p_d(s) & 0 \\ 0 & 0 & \cdots & 0 & q_1(s) \\ \vdots & \vdots & \ddots & \vdots & \vdots \\ 0 & 0 & \cdots & 0 & q_d(s) \\ 0 & 0 & \cdots & 0 & 1 \end{bmatrix}, \quad (14)$$

it can be shown by induction (Appendix A.2) that the product of these matrices yields the count of constraint violations in the top-right corner of the resulting matrix:

$$[1 \ 0 \ 0] \left(\prod_{n=1}^N M(s_n) \right) \begin{bmatrix} 0 \\ 0 \\ 1 \end{bmatrix} = \sum_{n=1}^{N-1} \eta(s_n, s_{n+1}). \quad (15)$$

This matrix form is similar to the treatment of operators in [132, 135]. To retrieve the penalty in MPO form, we can add Kronecker deltas analogously to before.

We have therefore found an MPO representation of a penalty term to the loss function Hamiltonian that can enforce a nearest-neighbor constraint. As presented in the appendix (appendix A.3), MPO representations for the other constraints in section 3.3 can be constructed with similar methods to how we constructed the MPO representations for the loss function Hamiltonian and the nearest-neighbor constraint.

5 Numerical Demonstration

For a numerical demonstration of our quantum representation of the stacking sequence retrieval problem, outlined in section 3, we implemented the MPO derived in section 4.2. We then conducted several computational trials using the DMRG algorithm, in order to optimize for the ground state of the Hamiltonian. This ground state corresponds to the optimal solution of the stacking sequence retrieval problem. As for manufacturing constraints, we implemented the symmetry constraint directly into the state representation and a disorientation constraint as a penalty, as outlined in section 3.3. The latter was included in the MPO form from section 4.3. The numerical trials were performed with a variety of different settings in the DMRG algorithm, giving first insights into the characteristics of our approach.

5.1 Setup

The numerical calculations were performed on a laptop equipped with an Intel Core i7-1185G7 processor (4 cores, 3.00 GHz), 16GB RAM, running Windows 10 Professional. The numerical implementation and trials were carried out in the programming language *Julia* version 1.8.4. The MPS and MPO were implemented by utilizing the *ITensors.jl* library in version 0.3.22 [136, 137], which also provided an implementation of the DMRG algorithm. Since this implementation of DMRG only supports alternating sweeping directions, we therefore modified the algorithm to support custom sequences in the sweeping direction. We also added some additional functionality for recording data during the optimization. However, apart from the support for custom sweeping directions, the optimization itself remains unchanged compared to *ITensors*' original implementation. The complete code for the experiments can be found at [138]. The algorithm was executed on the CPU, without employing parallelization techniques like multi-threading. All generated files from our experiments can be found in HDF5 format at [139].

By leveraging the DMRG algorithm, we were able to perform stacking sequence retrieval for a symmetric laminate comprising 400 plies. A ply count of this magnitude is at the higher end of the spectrum of what is common in the industry, and can be found in some large-scale structural designs [140–142]. Since the laminate is symmetric, we only modeled the upper half of the stack, consisting of $N = 200$ plies, and utilized the lamination parameters for symmetric laminates as defined in eq. (8). The ply orientations employed were the commonly used $d = 4$ angles:

$$\theta_1 = 0^\circ, \quad \theta_2 = +45^\circ, \quad \theta_3 = 90^\circ, \quad \theta_4 = -45^\circ.$$

We incorporated a disorientation constraint limiting the ply-angle difference between neighboring plies to 45° or less. This constraint is violated when neighboring plies are θ_1 and θ_3 , or θ_2 and θ_4 . The MPO for the penalty, as detailed in section 4.3, consists of site tensors based on vectors $\vec{p}(s)$ and $\vec{q}(s)$. Following eq. (13), these take the form:

$$p_k(s) = \delta_{k,s}, \quad q_k(s) = \gamma(\delta_{k,s+2} + \delta_{k,s-2}),$$

where γ represents the penalty added for a single constraint violation. From previous tests, it was observed that the algorithm predominantly finds solutions with a loss function value below 0.001. Keeping this in mind, we set the penalty at $\gamma = 0.005$. All trials of the DMRG algorithm were performed with and without including the constraint.

For selecting a well-justified set of target lamination parameters, we considered two key factors. Firstly, we opted for target parameters that correspond to exact solutions of feasible stacking sequences. This approach allows the loss function to serve as an effective quality measure for any obtained solution, since an optimal solution with the minimal loss function value of 0 always exists. We can obtain suitable target parameters from randomly generated stacking sequences that comply with the constraints, such that these stacking sequences simultaneously act as known optimal solutions the target parameters. Secondly, it is important that the target lamination parameters represent a diverse cross-section of potential lamination parameters. Common methods for generating random stacking sequences often result in density variations within the corresponding point cloud in the 8-dimensional lamination parameter space, which typically arise from the specifics of the sequence generation method. To counteract potential biases from our random generation method, we created a large dataset of 500,000 stacking sequences that adhere to the disorientation constraint, which were then translated into an equivalent number of points in lamination parameter space. We then employed a kernel density estimator to assess the point density at each location [143–145]. Finally, we utilized the inverses of these densities as weights to randomly select points in a manner that more closely resembles a uniform distribution across the lamination parameter space. With this method, we sampled a set of 50 target lamination parameters that we used for all our trials.

The DMRG algorithm offers flexibility in its configuration, allowing for various operational settings (Table 1). For example, standard implementations of DMRG enable control over the MPS bond dimension, as described in section 4. Opting for a higher maximum bond dimension facilitates the representation of a wider array of states, which can capture longer range correlations between distinct parts of the system and hence may lead to better solutions. However, this benefit is balanced against longer run times of the algorithm. To assess the DMRG's performance in terms of solution quality and computational time, we explored maximum bond dimensions of 2, 4, 8, 16, and 32 in our trials.

Another aspect of DMRG's configurable nature concerns the algorithm's operational sequence. As described in section 4, DMRG operates by performing sweeps of local optimizations over the entire MPS,

number of plies N (one half of symmetric laminate)	200
ply-angles	$0, +45^\circ, 90^\circ, -45^\circ$
constraints	symmetry constraint, with and without disorientation constraint of 45°
maximum bond dimension	2, 4, 8, 16, 32
sweep direction	to left alternating to right
number of trials per configuration	5

Table 1: Overview of the different settings employed in our trials.

and consistently initiating sweeps from the same end of the MPS requires an additional gauging step in between sweeps. In our study, we evaluated the algorithm’s performance using different sweeping strategies: sweeping only to the right (from the middle of the laminate $n = 1$, to the outside $n = N$), only to the left (from the outside of the laminate inward), and alternating sweep directions. We monitored the optimization progress by recording the expectation value of the loss function Hamiltonian before the start of the optimization and after each sweep. Each optimization was conducted for 69 sweeps, resulting in a total of 70 data points for each trace. Additionally to tracing the expectation value of the Hamiltonian, we recorded the time duration of each sweep, in order to investigate the dependence of the runtime on the individual configurations of the DMRG algorithm.

Further flexibility is given with the selection of an initial MPS at the start of the optimization process. For each of the 50 target lamination parameters, we randomly generated 5 distinct MPS, each with a constant bond dimension of 2. These initial MPS were consistently used across all trials with different bond dimensions and sweeping sequences. Given that this initial bond dimension is lower than most of the chosen maximum bond dimensions, the bond dimension of the MPS increases during the initial sweeps of the optimization until it reaches the predetermined maximum bond dimension. Therefore, most of the sweeps take place with the maximum bond dimension.

In the final stages of the optimization, we implemented a technique to enforce a basis state corresponding to a single stacking sequence. This involved successively halving the maximum bond dimension during the last few sweeps, ultimately reaching a bond dimension of 1 in the second to last sweep. In the last sweep, we applied a truncation criterion, which omits singular values below 0.5 during the dimension reduction, effectively ensuring the enforcement of a basis state.

Besides these specific configurations, we retained the default settings in ITensors for other aspects of the DMRG algorithm.

5.2 Numerical results

In this section we discuss the main results from all trials of the DMRG algorithm for stacking sequence retrieval. When the disorientation constraint was included, we confirmed that all resulting stacking sequences were free of any constraint violations. This observation suggests that the penalty parameter γ was set sufficiently high.

As outlined in the previous section, we recorded the expectation value of the loss function Hamiltonian after each sweep in all trials. Figure 4 presents the average across all target lamination parameters as a function of the number of sweeps. Each trace corresponds to a different configuration in terms of bond dimension, sweeping direction, and the inclusion or exclusion of the disorientation constraint. In all configurations, there is a rapid decrease in the expectation value during the initial sweeps, followed by a significant slowdown in the optimization rate. For configurations with alternating sweeps, this initial phase

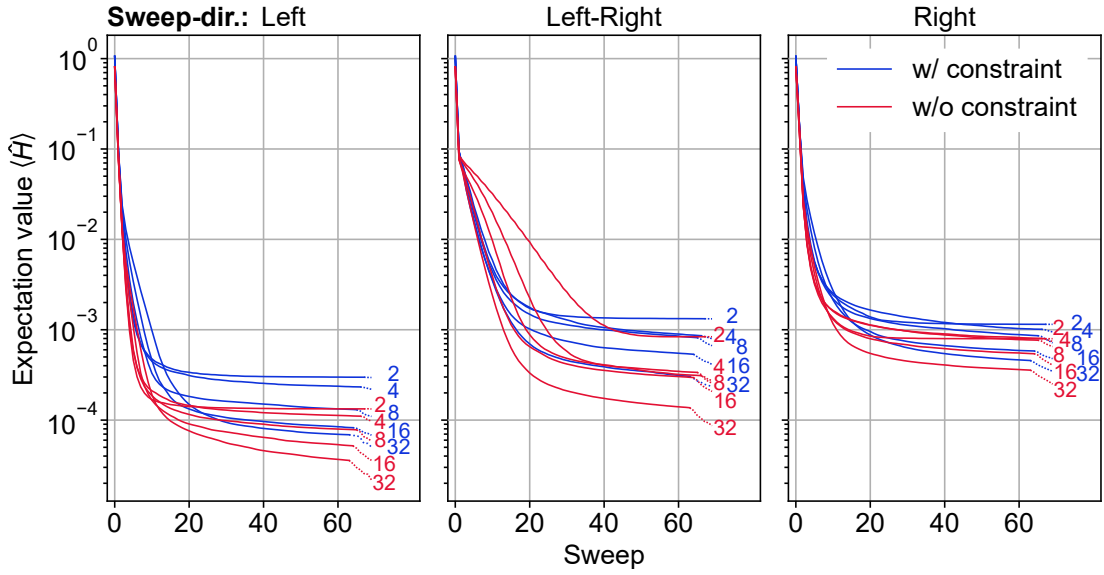


Figure 4: Traces of expectation values of the loss function Hamiltonian, averaged over all samples and measurements after each sweep. Each line corresponds to a different bond dimension, denoted at the end of each trace. Red lines represent trials excluding the disorientation constraint and blue lines correspond to trials including the constraint. Solid lines represent the optimization phase with a constant maximum bond dimension. The successive reduction of the bond dimension at the final phase of the optimization is indicated by dotted lines that can be found at the right-hand end of each trace.

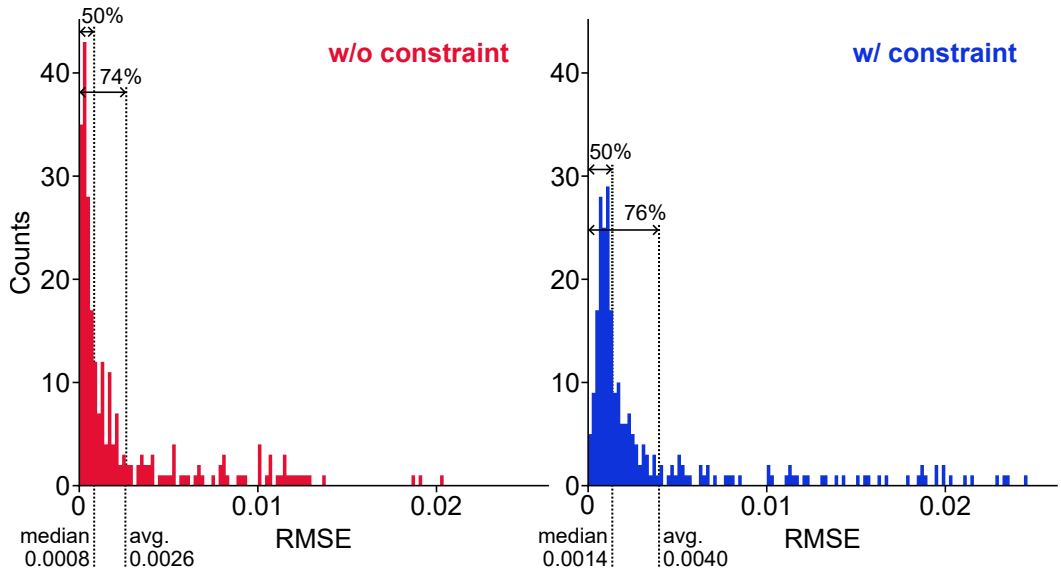


Figure 5: Histogram of the RMSE of the solutions for maximum bond-dimension 32 and left-sweeping direction. Counted were the points from all target lamination parameters and initial MPS. The bin-size is 0.002. The ranges of RMSE for the bottom half of the points, and up to the average RMSE are shown in both plots. Left: Without the disorientation constraint. Right: With the disorientation constraint.

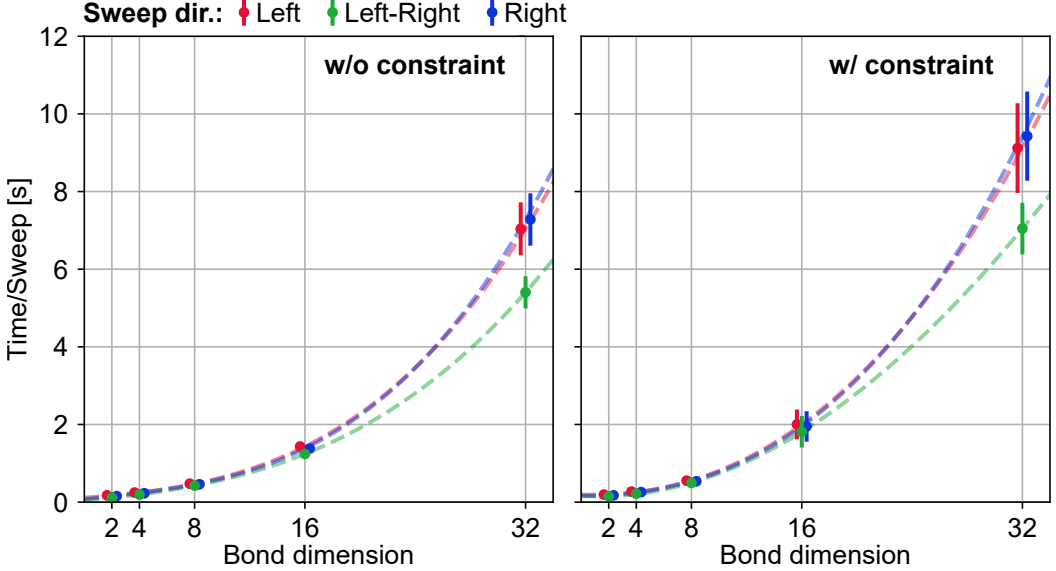


Figure 6: Average sweep duration as a function of bond dimension. Left and right plots respectively correspond to scenarios without and with the disorientation constraint. Each sweep direction is represented by distinct points in different colors. A third-order polynomial fit is included as dashed lines, to easier distinguish trends for different configurations.

of rapid optimization is less pronounced. Generally, larger bond dimensions yield better performance, as indicated by lower expectation values of the loss function. As anticipated, the algorithm achieves lower values without the disorientation constraint compared to when including the constraint. In terms of sweep direction, sweeping to the right (outward) shows less favorable results, while sweeping to the left (inward) outperforms alternating sweeps. This pattern suggests that optimizing the outer layers of the stack first, which influence both the A - and D -lamination parameters, before moving to the middle layers, where the impact on the D -parameters is minimal, is advantageous. The reduction in bond dimension, indicated by the dotted lines at the end of each trace in Figure 4, leads to a pronounced reduction in the expectation value of the loss function. This indicates that just before this reduction, the MPS represents a superposition of basis states that includes less optimal states, which are then filtered out during the bond dimension reduction.

While the averaged traces provide an overview, they do not reveal the actual distribution of all resulting lamination parameters for each specific configuration. A more nuanced understanding is gained by analyzing the distributions of the results for each configuration. For example, Figure 5 displays histograms of the RMSE across all samples for the most effective configuration (bond dimension 32 and sweeping to the left) with and without the disorientation constraint. The bin size of the histograms is set to 0.002. The histogram demonstrates how the majority of the trial significantly outperform the worst. Without the disorientation constraint, the median RMSE of all results is approximately 4.1% of the worst result's RMSE; with the constraint, it rises to about 6%. This skew in distribution means that in both scenarios, roughly three-quarters of the results fall below the average RMSE. These observations indicate that although the worst data points affect the average, a significant portion of the trials yield considerably better results.

A detailed overview of the results of all individual trials can be found in Figure 7 in Appendix A.6. An additional insight from these data points is that the quality of solutions for the same target parameters does not consistently correlate across different configurations. For instance, some data points that perform well with leftward sweeps may rank among the worst with rightward sweeps, and vice versa. This means that although leftward sweeps on average perform notably better than rightward sweeps, this might not be the case for a specific target lamination parameters. Similarly, results that excel without the disorientation constraint can show a marked decline in performance when the constraint is applied. Notably, in cases involving the disorientation constraint, there are often significantly larger discrepancies between the best and worst outcomes for a specific configuration. This variation suggests that the inclusion of the constraint potentially increases the sensitivity of the optimization process to the initial MPS.

Along with the expectation value of the loss function, we also tracked the time duration of each sweep.

Figure 6 illustrates the average duration of sweeps as a function of the bond dimension. This figure includes separate traces to distinguish between different sweeping directions and to compare the cases with and without the disorientation constraint. For calculating the averages and standard deviations, the first and last 10 sweeps were omitted. Further, to mitigate the impact of background processes of the computer’s operating system on the duration of isolated sweeps, the lowest and highest 10% of the times for all considered sweeps were also excluded. In the DMRG algorithm, the most computationally intensive step involves finding the eigenvector with the lowest eigenvalue of a matrix, which is a crucial part of the local optimizations of the site tensors. The computational complexity for solving the eigenvalue problem generally scales as $O(b^3)$, where b is the bond dimension. This scaling behaviour is also present in the Lanczos algorithm, which is employed for the eigenvalue computations, provided that the number of non-zero elements in the matrix scales in proportion to its overall size. The increased runtime for larger bond dimensions is clearly observable in Figure 6. However, given the limited number of data points for different bond dimensions, we cannot make firm assertions about the actual observed scaling behavior. Nevertheless, for illustrative purposes, we have included a third-order polynomial fit in the figure to facilitate easier comparison of the different configurations.

As noted in section 4, consistently initiating sweeps from the same side necessitates an extra gauging step between each sweep. This requirement is reflected in the marginally longer runtimes for such configurations compared to those with alternating sweeps, as seen in Figure 6. The inclusion of the disorientation constraint also results in increased runtimes. This can be attributed to the additional term in the Hamiltonian, which specifically affects tensor contractions during execution of the algorithm. However, this term should not significantly impact the dominant eigenvalue problem in local optimizations, as the size of the environment tensor involved in finding its eigenvector remains the same even when the constraint is added.

5.3 Discussion

Our numerical study provides valuable validation for our quantum representation of the stacking sequence retrieval problem, as outlined in section 3. The DMRG algorithm’s ability to heuristically approximate solutions, while generally not pinpointing the exact optimal one, confirms the efficacy of the Hamiltonian representation developed.

A key insight from our trials is the significant tradeoff between accuracy and runtime, particularly influenced by the bond dimensions. Higher bond dimensions are capable of capturing longer-range correlations and generally yield more accurate results, but at notably larger computational costs. This tradeoff is not unique to DMRG but also has broad implications for quantum algorithm development. In particular, proposed implementations of matrix product states as shallow-depth variational quantum circuits can potentially help mitigate the issue of the bond-dimension being a prohibitive factor in performance [146–148]. Furthermore, there is some indication, that quantum computers can improve upon results obtained from a classical calculation with MPS [149]. A quantum analog of the DMRG algorithm and other quantum algorithms might therefore be capable of achieving significantly higher accuracy. However, it should be noted, that the effectiveness of quantum algorithms like variational quantum algorithms can be inhibited by the resulting increase in parameters requiring optimization [150, 151].

The DMRG algorithm’s sensitivity to translational asymmetry in the weights of D -lamination parameters, as well as its response to different initial MPS configurations, yields important insights for broader quantum computing strategies. While the use of sweeping directions is unique to DMRG, it exemplifies how specific structural aspects, like translational asymmetry, can influence the performance of quantum algorithms. For example, to address difficulties in the variational optimization of parameterized quantum circuits, methods have been proposed that optimize parts of the quantum circuits sequentially [152, 153]. This resembles how DMRG performs local optimizations, and the superior performance of moving towards the middle of the laminate over moving outward might also be present with these methods. Another parallel of variational quantum algorithms to our DMRG implementation is the selection of initial parameters. Similar to how the initial MPS had an impact on the performance of the DMRG algorithm, the often randomly generated initial parameters in a quantum circuit play a significant role in the success of the optimization [150, 154–156]. Acknowledging this impact highlights the need for adaptive strategies, including multiple trials, to effectively navigate these inherent uncertainties.

Moreover, most target parameters significantly outperform the worst cases, and the results indicate

a dependency on the specific configuration used, especially the sweeping direction and initial MPS. For those cases that perform poorly, a different configuration may yield better results. One might therefore consider specialized strategies, such as warm-starting [157, 158], by conducting initial trials with smaller bond dimensions and then, for suboptimal results, selectively re-running the algorithm with adjustments. These adjustments might include increasing the bond dimension, experimenting with different sweeping directions, or opting for alternative initial MPS configurations.

The inclusion of the disorientation constraint in our DMRG trials, while leading to a modest reduction in accuracy, aligns with the algorithm’s strength in handling nearest-neighbor interactions. This naturally raises considerations about DMRG’s adaptability to constraints that introduce long-range couplings, such as the contiguity constraint or the 10%-rule (section 3.3). In this context, alternative tensor network structures like tree tensor networks [159] or MERA [160], known for their ability to capture long-range interactions, may offer potential solutions. However, these structures necessitate more complex and resource-intensive optimization methods, and their feasibility as viable alternatives to existing methods needs further investigation. Similarly, quantum algorithms, particularly variational quantum algorithms, present adaptability through their circuit designs, which could potentially accommodate long-range interaction considerations more efficiently than classical tensor network methods. The success of these quantum algorithms, however, is heavily influenced by the specific architecture of the quantum computers used, especially the connectivity between qubits. As such, the architecture and connectivity inherent to a quantum computing platform play a crucial role in determining the viability of quantum algorithms for addressing complex constraints in stacking sequence retrieval.

Considering the practical aspects of our research approach, it is crucial to highlight that our numerical trials were conducted using the DMRG method, based on the implementation provided by the *ITensors.jl* library, on a CPU without optimizing for performance. Implementing parallelization techniques, GPU support, sparse matrix optimizations, or problem-specific methods could lead to substantial performance enhancements. Additionally, adjusting other DMRG settings, such as hyperparameters in the eigenvalue solver, might further impact performance.

In conclusion, our study lays the groundwork for further investigation into the potential of DMRG as a viable alternative for stacking sequence retrieval. To achieve this, it is essential to incorporate the specific manufacturing constraints discussed earlier, such as the contiguity constraint and the 10%-rule, which are crucial for real-world applications [38–40]. Alongside these additions, implementing performance enhancements such as parallelization, GPU support, and optimization of algorithm settings is critical for this method to be competitive with existing stacking sequence retrieval techniques. Nevertheless, the results from our study offer encouraging signs that tensor networks and quantum algorithms could play a significant role in advancing quantum and quantum-inspired methods for laminate design.

6 Conclusions and Outlook

In this paper, we have taken crucial steps towards implementing quantum computing methods for tackling the stacking sequence retrieval problem, a significant challenge in the field of laminated composite design.

We began by developing a quantum representation of the stacking sequence retrieval problem, making it suitable for quantum computing methods. Initially, the problem was formalized as an integer optimization problem, where ply-angle sequences were represented as a list of integers, and the loss function quantified the mean square error between the lamination parameters of a given configuration and the target parameters. These stacking sequences were then embedded in a Hilbert space, with each basis state corresponding to a distinct stacking sequence. Subsequently, a Hamiltonian, embodying the loss function as a hermitian operator, was derived. We examined various manufacturing constraints and their implementation as penalty terms in the loss function. The translation of these penalty terms into operators within the Hamiltonian showed varied forms of subsystem interactions for individual plies.

In the second part of our study, we conducted numerical simulations to validate our approach. The DMRG algorithm, a classical tensor network method for finding the ground state of quantum lattice systems, was central to these simulations. The Hamiltonian for our problem, including a penalty term for the disorientation constraint, was represented in matrix product operator form. In our computational trials, we applied the DMRG algorithm to a set of 50 target lamination parameters, varying configurations in maximum bond dimension, sweeping direction, and the inclusion or exclusion of the disorientation constraint. The algorithm was able to successfully retrieve approximate solutions to the SSR problem

respective target parameters. Furthermore, these simulations demonstrated a clear tradeoff between accuracy and computational time related to the bond dimension. The sweeping direction also played a crucial role in determining the accuracy of results, stemming from the translational asymmetry in how individual ply-orientations affect the D -lamination parameters. The initial MPS selected at the beginning of the optimization process also influenced the accuracy of the outcomes. Including the disorientation constraint slightly reduced accuracy on average. Nevertheless, the algorithm produced approximate solutions that respect the constraint and hence validated the use of penalty terms to enforce manufacturing constraints.

As we lay the foundation for stacking sequence retrieval with quantum methods, our work gives rise to a spectrum of research opportunities. As discussed, the penalty terms for the various manufacturing constraints differ considerably in their composition, which in turn is expected to significantly affect the efficacy of different quantum algorithms and their suitability with various quantum hardware architectures. Identifying quantum algorithms that effectively respond to these constraints and exploring the impact of these constraints on algorithm performance across a range of quantum computing platforms remains a topic for further research. Beyond the integration of penalty terms, alternative approaches in handling constraints within quantum algorithms present a rich area for exploration. Some quantum algorithms might inherently produce superpositions of states adhering to specific constraints, like variational quantum algorithms where the circuit structure could intrinsically satisfy certain conditions. Conversely, if quantum algorithms struggle with certain constraints, alternative enforcement methods might be necessary. For instance, in classical approaches like permutation genetic algorithms the ratios of the ply-angles are predetermined [161], such that the constraint for balanced laminates and the 10% rule are already satisfied. Our approach to translating the problem into a quantum setting, while straightforward, is not the only possibility. Other representations, like choosing a different basis in Hilbert space, could offer more natural enforcement of constraints or align better with specific quantum algorithms, warranting further exploration. In real-world applications, a notable area yet to be investigated is how our approach can be adapted to scenarios involving multiple panels, each with distinct stacking sequences and lamination parameters. These situations often require adherence to blending rules, which govern the relationship between neighboring stacking sequences, introducing an added layer of complexity. Future research will need to address how to extend our quantum mechanical representation to accommodate these blending rules and how different approaches might enforce or utilize them in a quantum computing context. Exploring and implementing these extensions effectively constitutes an important area of ongoing research.

Our numerical simulations offer promising indications for the use of quantum computing and tensor networks in stacking sequence retrieval, though much remains to be explored. A critical aspect is the integration of additional manufacturing constraints, vital for real-world applications, and evaluating whether the DMRG algorithm can efficiently handle these complexities. Moreover, the implementation of performance optimizations will be crucial in assessing whether this approach can rival existing classical methods in efficacy. Furthermore, when considering scenarios involving multiple panels, the one-dimensional structure of MPS and DMRG becomes less applicable. Future investigations will need to explore whether alternative tensor network structures and optimization methods can offer advantages over traditional methods in such multi-panel contexts.

Our exploration into the application of quantum computing for stacking sequence retrieval, particularly the process of selecting optimal sequences from a set of discrete choices, may have implications beyond laminated composite design. For example, the definition of the lamination parameters in section 2.2 resembles the weighted-sum model in multi-criteria decision making, which is employed in a variety of applications [162–164]. This suggests that the methodologies and insights gained from our study can potentially inform approaches to quantum computing in other domains, thereby contributing to the progress in the practical application of quantum computational methods.

In conclusion, this research establishes a foundation for a further exploration into the utility of quantum algorithms for stacking sequence retrieval and laminate design, by developing a quantum representation of the problem. Moreover, we introduced tensor networks as a potential quantum-inspired approach. Importantly, our numerical results substantiate the efficacy of our methods, and provide valuable insights into benefits and drawbacks of quantum and quantum-inspired methods for stacking sequence retrieval. Continued research is crucial to fully understand the role these advanced computational techniques might play in the future of laminate design.

Notation

Variables and indices

N	number of plies,
n	number of corresponding subsystems
	index over plies,
	index of corresponding subsystem
ϕ_n	ply-angle of ply n (not limited to discrete angles in Θ)
d	number of valid ply angles,
	dimension of subsystems
$\Theta = \{\theta_1, \dots, \theta_d\}$,	valid ply angles
s	index of ply angle $\theta_s \in \Theta$, $s \in \{1, \dots, d\}$,
	state of corresponding subsystem
\mathcal{S}	set of all stacking sequences, $\mathcal{S} = \{1, \dots, d\}^N$
$\vec{s} = (s_1, \dots, s_N)$	integer representation of a stacking sequence, $\vec{s} \in \mathcal{S}$
t, t', t_1, t_2, \dots	summation indices for ply angle indices or states akin to s or s_n ,
	selected states for constraints
$\vec{t} = (t_1, \dots, t_N)$	summation index for stacking sequences akin to \vec{s}
$\vec{\theta} = (\theta_{s_1}, \dots, \theta_{s_N})$	ply angle sequence corresponding to \vec{s}
$v_1^A, v_2^A, v_3^A, v_4^A$	in-plane lamination parameters
$v_1^B, v_2^B, v_3^B, v_4^B$	coupling lamination parameters
$v_1^D, v_2^D, v_3^D, v_4^D$	out-of-plane lamination parameters
X	index of lamination parameters v_l^X
	for in-plane, coupling or out-of-plane $X \in \{A, B, D\}$
l	integer index of lamination parameters v_l^X ,
	index for corresponding objects like Γ_l or f_l ,
	usually $l = \{1, 2, 3, 4\}$
ξ_l^X	target value for lamination parameter v_l^X
f_l	functions in the calculation of the lamination parameters
	$f_1(s) = \cos(2\theta_s)$, $f_2(s) = \sin(2\theta_s)$, $f_3(s) = \cos(4\theta_s)$, $f_4(s) = \sin(4\theta_s)$
α^X	weights for the calculation of lamination parameter $v_l^X(\vec{s}) = \sum_{n=1}^N \alpha^X f_l(s_n)$
c	constraint $c : \mathcal{S} \rightarrow \{\text{True}, \text{False}\}$, $c(\vec{s}) = \text{False}$ iff. constraint is violated
H	loss function

Quantum notation

δ_{ab}	Kronecker-delta, $\delta_{ab} = 1$ if $a = b$, $\delta_{ab} = 0$ else
\mathcal{H}	Hilbert space (general),
	Hilbert space representing the complete stack, $\dim \mathcal{H} = d^N$
$\mathcal{L}(\mathcal{H})$	set of all linear maps (operators) on \mathcal{H}
\mathcal{H}_n	Hilbert space of subsystem n corresponding to ply n , $\dim \mathcal{H}_n = d$
$ \square\rangle$	vector in \mathcal{H} or its subsystems, e. g. $ \psi\rangle$
$ s\rangle$	basis vector of a subsystem Hilbert space corresponding to ply angle θ_s
$ \vec{s}\rangle = s_1 s_2 \dots s_N\rangle$	basis vector of full Hilbert space \mathcal{H} corresponding to stacking sequence \vec{s}
$\psi_{\vec{s}}, \psi_{s_1 s_2 \dots s_N}$	component of $ \psi\rangle$ for basis vector $ \vec{s}\rangle$ in decomposition $ \psi\rangle = \sum_{\vec{s}} \psi_{\vec{s}} \vec{s}\rangle$
$\langle \square $	dual of vector, e. g. $\langle \psi = \psi\rangle^\dagger$
$\langle \square \square \rangle$	inner product $\mathcal{H} \times \mathcal{H} \rightarrow \mathbb{C}$, e. g. $\langle \phi \psi \rangle$
$ \square\rangle \langle \square $	outer (dyadic) product $\mathcal{H} \times \mathcal{H} \rightarrow \mathcal{L}(\mathcal{H})$, e. g. $ \phi\rangle \langle \psi $, $(\phi\rangle \langle \psi) \chi\rangle = \langle \psi \chi \rangle \psi\rangle$
$\hat{\square}$	element in $\mathcal{L}(\mathcal{H})$ (operator on \mathcal{H} or its subsystems), e.g. \hat{A}
\square^\dagger	adjoint (conjugate transpose) of operator on \mathcal{H} , e. g. $\hat{A}^\dagger = (\hat{A}^*)^T$
\hat{H}	Hamiltonian, here linear operator in $\mathcal{L}(\mathcal{H})$ corresponding to loss function H
$\hat{H}_{X,l}$	term in \hat{H} the corresponding to loss with respect to lamination parameter v_l^X
$\square^{[n]}$	object defined for or acting on subsystem \mathcal{H}_n
$f_l^{[n]}$	operator corresponding to function f_l , acting on \mathcal{H}_n
$\hat{H}_{X,l}^{[n]}$	local operator on subsystem \mathcal{H}_n appearing in the Hamiltonian $\hat{H}_{X,l}$

H_c	penalty function for constraint c
\hat{H}_c	operator implementation of the penalty function H_c for constraint c
η	penalty function for a single constraint violation in the nearest-neighbor and k -local constraints

Tensor networks

$\psi_{\vec{s}} \equiv \psi_{s_1 \dots s_N}$	component of state $ \psi\rangle \in \mathcal{H}$ wrt. basis state $ \vec{s}\rangle = s_1 \dots s_N\rangle$, $\psi_{\vec{s}} = \langle \vec{s} \psi \rangle$
$A_{\vec{s}, \vec{s}'}$ $\equiv A_{s_1 \dots s_N, s'_1 \dots s'_N}$	matrix element of operator \hat{A} wrt. states $ \vec{s}\rangle = s_1 \dots s_N\rangle$ and $ \vec{s}'\rangle = s'_1 \dots s'_N\rangle$ $A_{\vec{s}, \vec{s}'} = \langle \vec{s}' \hat{A} \vec{s} \rangle$
$\psi_{s_n}^{[n]}$	local tensor at position n for MPS representation of state $ \psi\rangle$
$A^{[n]}$	local tensor at position n for MPO representation of operator \hat{A}
k_1, k_2, \dots	bond indices of an MPS or an MPO
$\psi_{s_n, k_{n-1} k_n}^{[n]}$	tensor elements of local tensor $\psi^{[n]}$ for site index s_n and bond indices k_{n-1}, k_n
$A_{s_n s'_n, k_{n-1} k_n}^{[n]}$	tensor elements of local tensor $A^{[n]}$ for site and bond indices s_n, s'_n and k_{n-1}, k_n
$h_{s_n}^{[n]}$	eigenvalue of local operator $\hat{H}_{X,l}^{[n]}$ wrt. local state s_n
$h_{\vec{s}} \equiv h_{s_1 \dots s_N}$	eigenvalue of partial Hamiltonian $\hat{H}_{X,l}$ wrt. state $ \vec{s}\rangle = s_1 \dots s_N\rangle$
$W_{s_n}^{[n]}$	matrix for local state s_n in matrix product decomposition $h_{\vec{s}} = W_{s_1}^{[1]} \dots W_{s_N}^{[N]}$
$W_{s_n s'_n}^{[n]}$	matrices for MPO representation of $\hat{H}_{X,l}$: $\langle \vec{s} \hat{H}_{X,l} \vec{s}' \rangle = W_{s_1 s'_1}^{[1]} \dots W_{s_N s'_N}^{[N]}$
$W_{s_n s'_n}^{[n]} = \delta_{s_n s'_n} W_{s_n}^{[n]}$	
\vec{p}, \vec{q}	vector used in the MPO representation of nearest-neighbor and k -local constraints

Author contributions

Arne Wulff: Conceptualization, Methodology, Formal Analysis, Investigation, Software, Data curation, Writing - original draft, Writing - review & editing, Visualization, Validation, **Boyang Chen:** Conceptualization, Writing - review & editing, Supervision, Funding acquisition, **Matthew Steinberg:** Methodology, Writing - review & editing, **Yinglu Tang:** Writing - review & editing, Supervision, Funding acquisition, **Matthias Möller:** Writing - review & editing, Supervision, Funding acquisition, **Sebastian Feld:** Writing - review & editing, Supervision, Funding acquisition

Code and data availability

The code for performing the experiments in section 5 can be found in a GitHub repository [138]. The generated data is available can be found in on 4TU.ResearchData [139].

Acknowledgements

We thank the remaining members of the QAIMS lab, Swapna Madabhushi Venkata, Koen Mesman and Philip Würzner, for valuable discussions regarding this work. We thank the Faculty for Aerospace Engineering at the Delft University of Technology for their funding support of the QAIMS lab.

Declaration of Interests

The authors declare that they have no known competing financial interests or personal relationships that could have appeared to influence the work reported in this paper.

Declaration of generative AI in scientific writing

During the preparation of this work the authors used OpenAI's ChatGPT exclusively for language suggestions and corrections. After using this service, the authors reviewed and edited the content as needed and take full responsibility for the content of the publication.

A Appendix

A.1 Terms in the penalty for the 10%-rule

In this section, we have a closer look into penalties to ensure the 10%-rule, as discussed in section 3.3. There, in eq. (10), we defined a possible penalty function to depend on the number of missing plies to satisfy the constraint:

$$H_{10\%-rule}(\vec{s}) = \begin{cases} 0, & \text{if } \sum_{n=1}^N \delta_{s_n, t} \geq N_t, \\ p\left(N_t - \sum_{n=1}^N \delta_{s_n, t}\right), & \text{else,} \end{cases}$$

where N_t is the minimum required number of plies with state t .

An intuitive approach to construct a suitable penalty function stems from the following realization: If the constraint is violated, then there exists at least one subset with $N - N_t + 1$ plies, that does not include any plies of state t . We can therefore simply define a suitable penalty function by checking all subsets of $N - N_t + 1$ plies and add a penalty, if no plies with state t are present. For example, if we denote the set of all k -element subsets of $\{1, \dots, N\}$ with $C(N, k)$, we can define the penalty function as:

$$H_{10\%-rule}(\vec{s}) = \sum_{\Lambda \in C(N, N - N_t + 1)} \prod_{n \in \Lambda} (1 - \delta_{s_n, t}).$$

Here, $(1 - \delta_{s_n, t}) = 1$ exactly if ply n is not in state t , $s_n \neq t$, and otherwise the expression is 0. For the terms, we thus add a penalty $\prod_{n \in \Lambda} (1 - \delta_{s_n, t}) = 1$, exactly if for all plies $n \in \Lambda$ we have $s_n \neq t$. Since this definition is symmetric under permutations of the plies, and therefore the result only depends on the difference in the number of current and required plies in state t , it represents a concrete example of the penalty function in eq. (10). Furthermore, the individual terms translate to operators on $N - N_t + 1$ subsystems in the quantum representation.

As discussed in section 3.3, these high-order operators can act unfavorably in certain quantum algorithms, especially those that require implementing the Hamiltonian as operations on the qubits. The question now is: Can we do better? As we show in this section, this is unfortunately not the case.

First, we will show, that a penalty function, as defined in eq. (10), will necessarily lead to terms of order $N - N_t + 1$. However, this definition is already somewhat restrictive, as it only allows penalty functions, that are symmetric under the permutation of the plies. From an optimization point of view, it makes sense that states with the same discrepancy to satisfying the constraint produce the same penalty. However, there might be penalty functions, that are not symmetric under permutation, but might be implementable with lower-order operators. In the final part of this section, we will show that any suitable operator for the 10%-rule will require operators acting on at least $N - N_t + 1$ subsystem, regardless of symmetry considerations.

A.1.1 Using the defined penalty function in eq. (10)

In this section, we show, that a decomposition into local operators of the penalty function for the 10%-rule, as defined in eq. (10) in section 3.3:

$$H_{\text{penalty}}^{10\%-rule}(\vec{s}) = \begin{cases} 0, & \text{if } \sum_{n=1}^N \delta_{s_n, t} \geq N_t, \\ p\left(N_t - \sum_{n=1}^N \delta_{s_n, t}\right), & \text{else,} \end{cases}$$

always includes terms of order $N - N_t + 1$.

For this purpose, we extend the definition of $p(x)$ also for valid states, where $x \geq N_t$. If we write $p(x)$ as a polynomial:

$$p(x) = \sum_{k=0}^{\deg p} a_k x^k,$$

– any other form would immediately yield a Taylor expansion up to infinite order – then each $x \in \{N_t, N_t + 1, \dots, N\}$ must be a root of the polynomial:

$$p(x) = 0.$$

Thus, since $p(x)$ has at least $N - N_t + 1$ roots, it must have at least an equivalent degree:

$$\deg p \geq N - N_t + 1.$$

For a state $\vec{s} \in \mathcal{S}$, we have:

$$x = N_t - \sum_{n=1}^N \delta_{s_n, t},$$

such that a power x^k yields:

$$\begin{aligned} x^k &= \left(N_t - \sum_{n=1}^N \delta_{s_n, t} \right)^k \\ &= (-1)^k \left(\sum_{n=1}^N \delta_{s_n, t} \right)^k + (-1)^{k-1} k N_t \left(\sum_{n=1}^N \delta_{s_n, t} \right)^{k-1} + (-1)^{k-2} \frac{1}{2} (k-1) k N_t^2 \left(\sum_{n=1}^N \delta_{s_n, t} \right)^{k-2} + \dots \end{aligned}$$

Furthermore:

$$\left(\sum_{n=1}^N \delta_{s_n, t} \right)^k = \sum_{n_1, \dots, n_k}^N \delta_{s_{n_1}, t} \delta_{s_{n_2}, t} \dots \delta_{s_{n_k}, t}.$$

Since $p(x)$ contains terms with $k = N - N_t + 1$, the penalty function includes terms with $\delta_{s_{n_1}, t} \delta_{s_{n_2}, t} \dots \delta_{s_{n_k}, t}$, which translate to operators $|tt \dots t\rangle \langle tt \dots t|_{n_1 n_2 \dots n_k}$. Therefore, the according Hamiltonian will have terms of order $N - N_t + 1$.

A.1.2 Any penalty function will include high-order terms

Above, we showed that the specified penalty function in eq. (10) leads to terms of order $N - N_t + 1$. However, the penalty function is inherently symmetric under permutations of the elements in a state $\vec{s} \in \mathcal{S}$. Here, we show that indeed any penalty function, regardless of symmetry considerations, must include terms of order $N - N_t + 1$ or larger.

First, we note that non-diagonal local operators produce off-diagonal elements when combined to higher operators. We can therefore focus on diagonal operators. Furthermore, these diagonal operators directly translate to Kronecker-deltas in the classical penalty function, as can be seen from the matrix element of the operator:

$$\langle s | \left(\sum_{r=1}^d c_r |r\rangle \langle r| \right) |s\rangle = c_s = \sum_{r=1}^d c_r \delta_{r,s}$$

where $r, s \in \{1, \dots, d\}$ are states on a single subsystems. We can therefore focus on expansions of the classical penalty function in terms of Kronecker-deltas.

In order to demonstrate that any penalty function for the 10%-rule requires at least $N - N_t + 1$ -order terms, we show that any penalty function with lower order will be insufficient. We accomplish this by considering a function that only includes terms of order up to $k = N - N_t$:

$$Z(\vec{s}) = \sum_{\Lambda \in \mathcal{P}_k(N)} \sum_{\vec{a} \in \{1, \dots, d\}^{|\Lambda|}} \zeta_{\Lambda, \vec{a}} \delta_{\vec{s}[\Lambda], \vec{a}},$$

where $\zeta_{\Lambda, \vec{a}} \in \mathbb{R}$ are the coefficients of the expansion. Here we used the following notation: $\mathcal{P}_k(N)$ is the power set of $\{1, \dots, N\}$, up to cardinality k :

$$\mathcal{P}_k(N) = \{\Lambda \subseteq \{1, \dots, N\} : |\Lambda| \leq k\}.$$

We use subsets $\Lambda \in \mathcal{P}_k(N)$ to select subsequence of elements s_n of the state \vec{s} for $n \in \{1, \dots, N\}$, which we denote with:

$$\vec{s}[\Lambda] = (s_{n_1}, s_{n_2}, \dots, s_{n_{|\Lambda|}}) \in \{1, \dots, N\}^{|\Lambda|},$$

where $\Lambda = \{n_1, n_2, \dots, n_{|\Lambda|}\}$ and $n_1 < n_2 < \dots < n_{|\Lambda|}$. With the Kronecker-delta:

$$\delta_{\vec{s}[\Lambda], \vec{a}} = \delta_{s_{n_1}, a_1} \delta_{s_{n_2}, a_2} \dots \delta_{s_{n_{|\Lambda|}}, a_{|\Lambda|}},$$

we match the selected states of \vec{s} to a defined vector $\vec{a} \in \{1, \dots, d\}^{|\Lambda|}$. In an operator representation, these Kronecker-deltas are converted into operators $|a_1 a_2 \cdots a_{|\Lambda|}\rangle \langle a_1 a_2 \cdots a_{|\Lambda|}|_{n_1 n_2 \cdots n_{|\Lambda|}}$. For our proof, we show that if this function $Z(\vec{s})$ has roots on all valid states, it will necessarily also have roots for at least one constraint-violating state, which makes it unsuitable as a penalty function.

Before we continue, we first note, that:

$$\delta_{s_n, \alpha} = \delta_{s_n, \alpha} \sum_{\beta=1}^d \delta_{s_{n'}, \beta} = \sum_{\beta=1}^d \delta_{s_n, \alpha} \delta_{s_{n'}, \beta},$$

from which follows, that terms with lower order can be converted into terms with higher order. Therefore, instead of allowing terms with up to order k in $Z(\vec{s})$, we can focus on $Z(\vec{s})$ containing only terms of exactly order k :

$$Z(\vec{s}) = \sum_{\Lambda \in C(N, k)} \sum_{\vec{a} \in \{1, \dots, d\}^{|\Lambda|}} \zeta_{\Lambda, \vec{a}} \delta_{\vec{s}[\Lambda], \vec{a}}, \quad (16)$$

where $C(N, k)$ denotes the set of all combinations of k object from $\{1, \dots, N\}$ without replacement:

$$C(N, k) = \{\Lambda \in \mathcal{P}(N) : |\Lambda| = k\}.$$

The valid states \vec{s} , with:

$$\sum_{n=1}^N \delta_{s_n t} \geq N_t = N - k,$$

must not add a penalty:

$$Z(\vec{s}) = 0,$$

which defines a system of linear equations in $\zeta_{\Lambda, \vec{a}}$ in eq. (16), for which the rows of the according matrix are given by the $\delta_{\vec{s}[\Lambda], \vec{a}}$. We will show, that there exists a state $\vec{r} \in \mathcal{S}$ with less than N_t occurrences of state t , and thus should add penalty, but evaluates to $Z(\vec{r}) = 0$. We do so, by showing, that $\delta_{\vec{r}[\Lambda], \vec{a}}$ can be written as a linear combination of $\delta_{\vec{s}[\Lambda], \vec{a}}$ with valid states \vec{s} .

For this purpose, we define vectors $\vec{w}^{(\Gamma)} \in \mathcal{S}$ containing only state t and another state $u \in \{1, \dots, d\}$ with $u \neq t$, where the last $N - k - 1$ elements are all t :

$$\vec{w}^{(\Gamma)} = \vec{x}^{(\Gamma)} \oplus (t, \dots, t).$$

Here, $\Gamma \in \mathcal{P}(k+1)$ is a subset of $\{1, \dots, k+1\}$ and $\vec{x}^{(\Gamma)} \in \{t, u\}^{k+1}$ is defined by:

$$x_n^{(\Gamma)} = \begin{cases} t, & \text{if } n \in \Gamma, \\ u, & \text{if } n \notin \Gamma. \end{cases}$$

We will show that $\delta_{\vec{r}[\Lambda], \vec{a}}$ for:

$$\vec{r} = \vec{w}^{(\emptyset)} = (u, \dots, u, t, \dots, t),$$

which contains $N - k - 1 = N_t - 1$ occurrences of t , is a linear combination of $\delta_{\vec{w}^{(\Gamma)}[\Lambda], \vec{a}}$ with $\Gamma \neq \emptyset$, such that $\vec{w}^{(\Gamma)}$ constraints at least $N - k = N_t$ occurrences of t .

For a given $\Lambda = \{n_1, n_2, \dots, n_k\} \in C(N, k)$ and $\vec{a} \in \{1, \dots, d\}^{|\Lambda|}$, we assume that $n_1, \dots, n_m \leq k+1$ and $n_{m+1}, \dots, n_k > k+1$. Then for any $\Gamma \in \mathcal{P}(k+1)$:

$$\delta_{\vec{w}^{(\Gamma)}[\Lambda], \vec{a}} = \delta_{x_{n_1}^{(\Gamma)}, a_1} \delta_{x_{n_2}^{(\Gamma)}, a_2} \cdots \delta_{x_{n_m}^{(\Gamma)}, a_m} \delta_{t, a_{m+1}} \cdots \delta_{t, a_k}.$$

Note that for \vec{r} , where $\Gamma = \emptyset$, we get:

$$\delta_{\vec{r}[\Lambda], \vec{a}} = \delta_{u, a_1} \cdots \delta_{u, a_m} \delta_{t, a_{m+1}} \cdots \delta_{t, a_k}. \quad (17)$$

If we sum the Kronecker-deltas for all $\vec{x}^{(\Gamma)}$ with the same number $\alpha = |\Gamma|$ of t , we obtain:

$$\sum_{\Gamma \in C(k+1, \alpha)} \delta_{\vec{w}^{(\Gamma)}[\Lambda], \vec{a}} = \delta_{t, a_{m+1}} \cdots \delta_{t, a_k} \sum_{\Gamma \in C(k+1, \alpha)} \delta_{x_{n_1}^{(\Gamma)}, a_1} \delta_{x_{n_2}^{(\Gamma)}, a_2} \cdots \delta_{x_{n_m}^{(\Gamma)}, a_m}.$$

We can evaluate the sum on the right site, by considering that $\vec{x}^{(\Gamma)}$, which has length $k+1$, has to match \vec{a} on the sites defined by n_1, \dots, n_m , and that $\gamma = \text{count}(t, (a_1, \dots, a_m))$ occurrences of t are already bound in \vec{a} . Therefore, we need to count all combinations, where we place $\alpha - \gamma$ instances of t on the remaining $(k+1) - m$ sites:

$$\sum_{\Gamma \in C(k+1, \alpha)} \delta_{\vec{w}^{(\Gamma)}[\Lambda], \vec{a}} = \delta_{t, a_{m+1}} \cdots \delta_{t, a_k} \binom{(k+1) - m}{\alpha - \gamma},$$

where the brackets on the right side denote the binomial coefficient.

Now, we calculate the sum of all these expressions for $\alpha = 1, 2, \dots, k+1$ with alternating signs:

$$\begin{aligned} & \sum_{\alpha=1}^{k+1} (-1)^{\alpha-1} \sum_{\Gamma \in C(k+1, \alpha)} \delta_{\vec{w}^{(\Gamma)}[\Lambda], \vec{a}} \\ &= \delta_{t, a_{m+1}} \cdots \delta_{t, a_k} \sum_{\alpha=1}^{k+1} (-1)^{\alpha-1} \binom{(k+1) - m}{\alpha - \gamma} \\ &= \delta_{t, a_{m+1}} \cdots \delta_{t, a_k} \sum_{\alpha=1-\gamma}^{k+1-\gamma} (-1)^{\alpha+\gamma-1} \binom{(k+1) - m}{\alpha} \\ &= \delta_{t, a_{m+1}} \cdots \delta_{t, a_k} (-1)^{\gamma-1} \sum_{\alpha=\max(0, 1-\gamma)}^{k+1-m} (-1)^\alpha \binom{(k+1) - m}{\alpha}, \end{aligned}$$

where in the second line, we shifted the index α and in the third line, we trimmed to index α to reflect, that the binomial coefficient vanishes for $\alpha < 0$ or $\alpha > (k+1) - m$. We distinguish two cases: If the number of t in (a_1, \dots, a_m) is non-zero, then the expression vanishes:

$$\begin{aligned} & \sum_{\alpha=1}^{k+1} (-1)^{\alpha-1} \sum_{\Gamma \in C(k+1, \alpha)} \delta_{\vec{w}^{(\Gamma)}[\Lambda], \vec{a}} \\ &= \delta_{t, a_{m+1}} \cdots \delta_{t, a_k} (-1)^{\gamma-1} \sum_{\alpha=0}^{k+1-m} (-1)^\alpha \binom{(k+1) - m}{\alpha} \\ &= 0, \end{aligned}$$

where we used the identity $\sum_{j=1}^n (-1)^j \binom{n}{j} = 0$. If (a_1, \dots, a_m) does not contain any t , then we need to make sure to include the term $\alpha = 0$, in order to use this identity:

$$\begin{aligned} & \sum_{\alpha=1}^{k+1} (-1)^{\alpha-1} \sum_{\Gamma \in C(k+1, \alpha)} \delta_{\vec{w}^{(\Gamma)}[\Lambda], \vec{a}} \\ &= \delta_{t, a_{m+1}} \cdots \delta_{t, a_k} (-1)^{\gamma-1} \sum_{\alpha=1}^{k+1-m} (-1)^\alpha \binom{(k+1) - m}{\alpha}, \\ &= \delta_{t, a_{m+1}} \cdots \delta_{t, a_k} (-1)^{\gamma-1} \left(\sum_{\alpha=0}^{k+1-m} (-1)^\alpha \binom{(k+1) - m}{\alpha} - (-1)^0 \binom{(k+1) - m}{0} \right) \\ &= \delta_{t, a_{m+1}} \cdots \delta_{t, a_k}, \end{aligned}$$

where in the last line, we included that the number of t in (a_1, \dots, a_m) vanishes in this case, $\gamma = 0$ and thus $(-1)^{\gamma-1} = -1$. We can summarize the results for the two cases as:

$$\sum_{\alpha=1}^{k+1} (-1)^{\alpha-1} \sum_{\Gamma \in C(k+1, \alpha)} \delta_{\vec{w}^{(\Gamma)}[\Lambda], \vec{a}} = \delta_{u, a_1} \cdots \delta_{u, a_m} \delta_{t, a_{m+1}} \cdots \delta_{t, a_k},$$

which is exactly $\delta_{\vec{r}[\Lambda], \vec{a}}$ in eq. (17):

$$\delta_{\vec{r}[\Lambda], \vec{a}} = \sum_{\alpha=1}^{k+1} (-1)^{\alpha-1} \sum_{\Gamma \in C(k+1, \alpha)} \delta_{\vec{w}^{(\Gamma)}[\Lambda], \vec{a}}.$$

Therefore $\delta_{\vec{r}[\Lambda], \vec{a}}$ is linear combination of $\delta_{\vec{w}[\Lambda]^{(\Gamma)}, \vec{a}}$. As a consequence, if we choose $\zeta_{\Lambda, \vec{a}}$ in eq. (16), such that $Z(\vec{w}^{(\Gamma)}) = 0$ for all valid states with $\Gamma \neq \emptyset$, then $Z(\vec{r}) = 0$ for the constraint violating state \vec{r} . Thus, a suitable penalty function $Z(\vec{s})$ can not be constructed with only terms of order less than $N - N_t + 1$. As a consequence, any penalty Hamiltonian will contain terms of order $N - N_t + 1$ or more.

A.2 Derivation of equation (15)

In order to derive equation (15), we introduce introduce a matrix $\tilde{M}(s, s', a)$ for convenience:

$$\tilde{M}(\vec{p}(s'), \vec{q}(s), a) = \begin{bmatrix} 1 & p_1(s') & \cdots & p_d(s') & a \\ 0 & 0 & \cdots & 0 & q_1(s) \\ \vdots & \vdots & \ddots & \vdots & \vdots \\ 0 & 0 & \cdots & 0 & q_d(s) \\ 0 & 0 & \cdots & 0 & 1 \end{bmatrix}.$$

where $a \in \mathbb{R}$ is some real value.

Note that $M(s) = \tilde{M}(s, s, a)$. If we multiply an instance of $M(s'')$ to $\tilde{M}(s, s', a)$, and consider $\eta(s, s') = \sum_{k=1}^d p_k(s)q_k(s')$, we obtain:

$$\tilde{M}(s, s', a)M(s'') = \tilde{M}(s, s'', a + \eta(s', s'')).$$

It follows by mathematical induction, that:

$$\prod_{n=1}^N M(s_n) = \tilde{M}\left(s_1, s_N, \sum_{n=1}^{N-1} \eta(s_n, s_{n+1})\right).$$

The surrounding vectors in equation (15) select for the top-right corner of the matrix, $\sum_{n=1}^{N-1} \eta(s_n, s_{n+1})$, which concludes the derivation.

A.3 An MPO representation of the remaining constraints in section 3.3

Here, we present how the remaining manufacturing constraints in section 3.3, namely the contiguity constraint, balanced laminates and the 10%-rule, can be translated into MPO form.

A.3.1 The contiguity constraint

For the contiguity constraint, we extend the approach for nearest-neighbor constraints discussed in section 4.3 to k -local constraints. This extension involves modifying the penalty function, which is now defined for a sequence of k subsystems. Specifically, the penalty function $\eta(s_n, s_{n+1}, \dots, s_{n+k-1})$ assigns a penalty of γ if the sequence $(s_n, s_{n+1}, \dots, s_{n+k-1})$ violates the constraint, and 0 otherwise. To represent this penalty function, we seek k vectors $\vec{p}^{(1)}(s), \dots, \vec{p}^{(k)}(s) \in \mathbb{C}^{\tilde{d}}$ for each ply angle $s \in \{1, \dots, d\}$ such that:

$$\eta(s_n, s_{n+1}, \dots, s_{n+k-1}) = \sum_{j=1}^{\tilde{d}} p_j^{(1)}(s_n) p_j^{(2)}(s_{n+1}) \cdots p_j^{(k)}(s_{n+k-1}).$$

Here, d is the number of allowed ply angles, and \tilde{d} , a positive integer, denotes the size of these vectors. For the specific case of the contiguity constraint, which penalizes k consecutive plies with the same ply-angle, we find an effective representation with $\tilde{d} = d$. The vectors are defined as:

$$p_j^{(1)}(s) = \cdots = p_j^{(k-1)}(s) = \delta_{js}, \quad p_j^{(k)}(s) = \gamma \delta_{js}, \quad (18)$$

where we chose γ to included $p_j^{(k)}(s)$. Other possibilities include multiplying γ to another vector or distribute it by multiplying $\gamma^{\frac{1}{k}}$ to each of the vector.

We extend the definition of the matrix $M(s)$, as outlined in eq. (14), to adapt it for the k -local scenario. This adaptation involves constructing a square matrix of dimension $\tilde{d}(k-1) + 2$. The vectors $\vec{p}^{(1)}(s)$

and $\bar{p}^{(k)}(s)$ are incorporated in the first row and last column respectively, similar to eq. (14). However, to cater to the k -local aspect, we integrate additional columns and rows. These new elements form a diagonal matrix $\text{diag}(\bar{p}^{(2)}(s), \dots, \bar{p}^{(k-1)}(s))$ of dimension $\tilde{d}(k-2)$, with the elements of vectors $\bar{p}^{(2)}(s)$ to $\bar{p}^{(k-1)}(s)$ listed sequentially along the diagonal. The resulting matrix $M(s)$ for the k -local case can thus be represented in block-matrix form as:

$$M(s) = \begin{bmatrix} 1 & (\bar{p}^{(1)}(s))^T & \mathbf{0} & 0 \\ \mathbf{0} & \mathbf{0} & \text{diag}(\bar{p}^{(2)}(s), \dots, \bar{p}^{(k-1)}(s)) & \mathbf{0} \\ \mathbf{0} & \mathbf{0} & \mathbf{0} & \bar{p}^{(k)}(s) \\ \mathbf{0} & \mathbf{0} & \mathbf{0} & 1 \end{bmatrix}.$$

In this matrix, $(\bar{p}^{(1)}(s))^T$ is a row vector and $\bar{p}^{(k)}(s)$ is a column vector, both of size \tilde{d} . The matrices $\mathbf{0}$ contain only zeros and are sized appropriately. Single-element matrices containing 0 or 1 are denoted in regular font weight. As in section 4.3, a product of matrices $M(s_1) \cdots M(s_N)$ counts the penalties for constraint violations in the top right corner:

$$[1 \ 0 \ \cdots \ 0] M(s_1) \cdots M(s_N) \begin{bmatrix} 0 \\ \vdots \\ 0 \\ 1 \end{bmatrix} = \sum_{n=1}^{N-k+1} \eta(s_n, \dots, s_{n+k-1}), \quad (19)$$

where the vectors surrounding the product select for the first row and last column. Following, the element-wise (or Hadamard) product of two vectors, \vec{a} and \vec{b} , is denoted by $\vec{a} \odot \vec{b}$, and is defined as:

$$(\vec{a} \odot \vec{b})_j = a_j b_j.$$

To illustrate this, consider the action of a single matrix $M(s)$ on a vector. For an arbitrary complex number $a \in \mathbb{C}$ and vectors $\vec{b}^{(j)} \in \mathbb{C}^{\tilde{d}}$ for $j = 1, \dots, k-1$, the matrix operation is given by:

$$M(s) \begin{bmatrix} a \\ \vec{b}^{(1)} \\ \vec{b}^{(2)} \\ \vdots \\ \vec{b}^{(k-2)} \\ \vec{b}^{(k-1)} \\ 1 \end{bmatrix} = \begin{bmatrix} a + \bar{p}^{(1)}(s) \cdot \vec{b}^{(1)} \\ \bar{p}^{(2)}(s) \odot \vec{b}^{(2)} \\ \bar{p}^{(3)}(s) \odot \vec{b}^{(3)} \\ \vdots \\ \bar{p}^{(k-1)}(s) \odot \vec{b}^{(k-1)} \\ \bar{p}^{(k)}(s) \\ 1 \end{bmatrix}.$$

In this operation, each vector $\vec{b}^{(j)}$ is elevated one position and then multiplied element-wise with the corresponding vector $\bar{p}^{(j)}(s)$. The top vector $\vec{b}^{(1)}$ undergoes a dot product with $\bar{p}^{(1)}(s)$, which is added to the scalar a . The vector $\bar{p}^{(k)}(s)$ is inserted into the bottom slot that becomes vacant. Consequently, when the matrices in equation (19) are multiplied from right to left, we observe the sequential accumulation and elevation of the vectors $\bar{p}^{(k)}$. This is depicted in the following process:

$$\begin{aligned} & \begin{bmatrix} 0 \\ \vdots \\ 0 \\ 1 \end{bmatrix} \xrightarrow{M(s_N)} \begin{bmatrix} 0 \\ \mathbf{0}_{\tilde{d}(k-2)} \\ \bar{p}^{(k)}(s_N) \\ 1 \end{bmatrix} \xrightarrow{M(s_{N-1})} \begin{bmatrix} 0 \\ \mathbf{0}_{\tilde{d}(k-3)} \\ \bar{p}^{(k-1)}(s_{N-1}) \odot \bar{p}^{(k)}(s_N) \\ \bar{p}^{(k)}(s_{N-1}) \\ 1 \end{bmatrix} \xrightarrow{M(s_{N-2})} \dots \\ & \xrightarrow{M(s_{N-k+2})} \begin{bmatrix} 0 \\ \bar{p}^{(2)}(s_{N-k+2}) \odot \dots \odot \bar{p}^{(k)}(s_N) \\ \vdots \\ \bar{p}^{(k-1)}(s_{N-k+2}) \odot \bar{p}^{(k)}(s_{N-k+3}) \\ \bar{p}^{(k)}(s_{N-k+2}) \\ 1 \end{bmatrix} \xrightarrow{M(s_{N-k+1})} \begin{bmatrix} \eta(s_{N-k+1}, \dots, s_N) \\ \bar{p}^{(2)}(s_{N-k+1}) \odot \dots \odot \bar{p}^{(k)}(s_{N-1}) \\ \vdots \\ \bar{p}^{(k-1)}(s_{N-k+1}) \odot \bar{p}^{(k)}(s_{N-k+2}) \\ \bar{p}^{(k)}(s_{N-k+1}) \\ 1 \end{bmatrix}. \end{aligned}$$

In this sequence, the suffixes of the matrices $\mathbf{0}$ indicate their size. Upon integrating the matrix $M(s_{N-k+1})$, the accurate penalty for the last k subsystems, from $N-k+1$ to N , is added to the first row. The

elements below are positioned to include the correct penalty for the subsystems from $N - k$ to $N - 1$ when the subsequent matrix $M(s_{N-k})$ is integrated into the product. By continuing this process for all matrices and then selecting the first row, the correct penalty for the entire stacking sequence \vec{s} is computed, validating equation (19).

The matrices resulting from this formulation, each having a dimension of $\tilde{d}(k - 1) + 2$, are notably larger compared to the other MPOs we have previously discussed. For instance, considering a contiguity constraint that limits consecutive plies of the same angle to a maximum of $N_{\text{same}} = 5$, making the constraint $k = 6$ -local, and with $d = 4$ ply angles (recalling that $\tilde{d} = d$ from eq. (18)), these matrices attain a dimension of $\tilde{d}(k - 1) + 2 = 22$. This dimension is significantly larger compared to the 2-dimensional MPO for lamination parameters and the 4-dimensional MPO for the nearest-neighbor constraint. However, in the DMRG algorithm, the matrix size impacting the most computationally intensive step – finding the lowest lying eigenvalue – depends only on the bond dimensions of the MPS and the number of potential states d of the subsystems. The bond dimension of the MPO mainly affects tensor contractions, which are anticipated to have a lesser impact on the algorithm’s runtime. Moreover, the matrices in the MPO for the constraint are predominantly sparse and have predictable patterns. This characteristic indicates that using specialized matrix multiplication algorithms for sparse matrices, or directly implementing the matrices’ effects on the tensor elements, could significantly enhance performance efficiency. While we expect a minimal impact on runtime, it remains to be seen how DMRG will navigate these intricate constraints and what implications they may have on the solution’s accuracy.

A.4 Balanced laminates

As outlined in section 3.3, the constraint for balanced laminates, as well as generalized constraints where two states, s and t , appear an equal number of times in a stacking sequence, can be expressed using a penalty operator:

$$\hat{H}_{\text{balanced}} = \gamma \left(\sum_{n=1}^N \hat{H}^{[n]} \right)^2,$$

where the local operators $\hat{H}^{[n]}$ are defined for each subsystem n as:

$$\hat{H}^{[n]} = |s\rangle\langle s|_n - |t\rangle\langle t|_n = \sum_{s_n=1}^d (\delta_{s_n,s} - \delta_{s_n,t}) |s_n\rangle\langle s_n|_n.$$

Given that the penalty operator bears similarity to the Hamiltonian form for the lamination parameters, as seen in eq. (5), the same methodology discussed in section 4.2 can be applied. For this, we set the eigenvalues $h_{s_n}^{[n]}$ of the system to:

$$h_{s_n}^{[n]} = \delta_{s_n,s} - \delta_{s_n,t},$$

yielding a representation of the penalty operator $\hat{H}_{\text{penalty}}^{(\text{balanced})}$ in MPO form. The factor γ can be included by multiplying it to any one of the local tensors.

A.5 The 10%-rule

As detailed in section 3.3, constraints such as the 10%-rule require a minimum of N_s plies to be in a specific state s . For this constraint, we implement a linear penalty function:

$$H_{10\%-rule}(\vec{s}) = \begin{cases} 0, & \text{if } \sum_{n=1}^N \delta_{s_n,s} \geq N_s, \\ \gamma \left(N_s - \sum_{n=1}^N \delta_{s_n,s} \right), & \text{else,} \end{cases},$$

where the parameter $\gamma > 0$ controls the magnitude of the added penalty. While an expansion of the according operator into single-site operators is more intricate, as discussed in section 3.3, a straightforward representation as an MPO can be found via the decomposition:

$$H_{10\%-rule}(\vec{s}) = [1 \ 0 \ \cdots \ 0] M(s_1) \cdots M(s_N) \begin{bmatrix} \gamma N_s \\ -\gamma \\ \vdots \\ -\gamma \end{bmatrix}, \quad (20)$$

where each $M(s_n)$ is a square matrix of dimension $N_s + 1$. For $s_n = s$, $M(s)$ is defined as:

$$M(s) = \begin{bmatrix} 1 & 1 & 0 & \cdots & 0 \\ 0 & 0 & 1 & \cdots & 0 \\ \vdots & \vdots & \ddots & \ddots & \vdots \\ 0 & 0 & \cdots & 0 & 1 \\ 0 & 0 & \cdots & 0 & 0 \end{bmatrix},$$

and for $s_n \neq s$, it is equivalent to the identity matrix:

$$M(s_n) = \mathbf{I}_{N_s+1} \quad \text{for } s_n \neq n.$$

Consequently, multiplying $M(s_n)$ with a vector $\vec{a} \in \mathbb{C}^{N_s+1}$ leaves \vec{a} unchanged if $s_n \neq s$. However, for $s_n = s$, it shifts all elements below the first row up by one position, combines the first two elements in the first row, and appends a zero at the end:

$$M(s) \begin{bmatrix} a_1 \\ a_2 \\ \vdots \\ a_{N_s+1} \end{bmatrix} = \begin{bmatrix} a_1 + a_2 \\ a_3 \\ \vdots \\ a_{N_s+1} \\ 0 \end{bmatrix}.$$

Thus, applying this matrix to the column vector in eq. (20) cumulatively adds $-\gamma$ for each occurrence of $s_n = s$, effectively subtracting from the penalty. If the constraint is satisfied for \vec{s} , the penalty becomes zero after N_s such additions. Meanwhile, the remaining elements of the vector are now also 0, such that multiplying any further matrices leave the vector unchanged. Conversely, if the constraint is not met, the penalty remains non-zero, reflecting the penalty function $H_{10\%-rule}(\vec{s})$. This justifies the decomposition in eq. (20), which can be used to construct the MPO similarly to previous cases in section 4.

As with the contiguity constraint discussed in section A.3.1, these matrices are larger than in other MPOs that we already encountered. For a 10%-rule in a laminate with $N = 200$ plies, requiring at least $N_s = 20$ plies in state s , we encounter matrices of dimension $N_s + 1 = 21$. Yet, as previously discussed, the dimension of the MPO has a comparatively minor impact on the DMRG algorithm's runtime, and there are opportunities to improve performance by exploiting the sparse structure of the matrices, or by directly implementing their predictable effects onto tensor elements. As before, the impact on the algorithm's accuracy remains to be explored.

A.6 Diagram of all measured samples

Figure 7 offers a tabular depiction of the outcomes of all measured samples. The rows and columns respectively represent different sweep directions and diverse bond dimensions. Here, the rows signify different sweep directions, and the columns represent the diverse bond dimensions, ranging from 2 to 32. The samples are sorted by the average values for bond dimension 32 and sweep direction left, without the constraint.

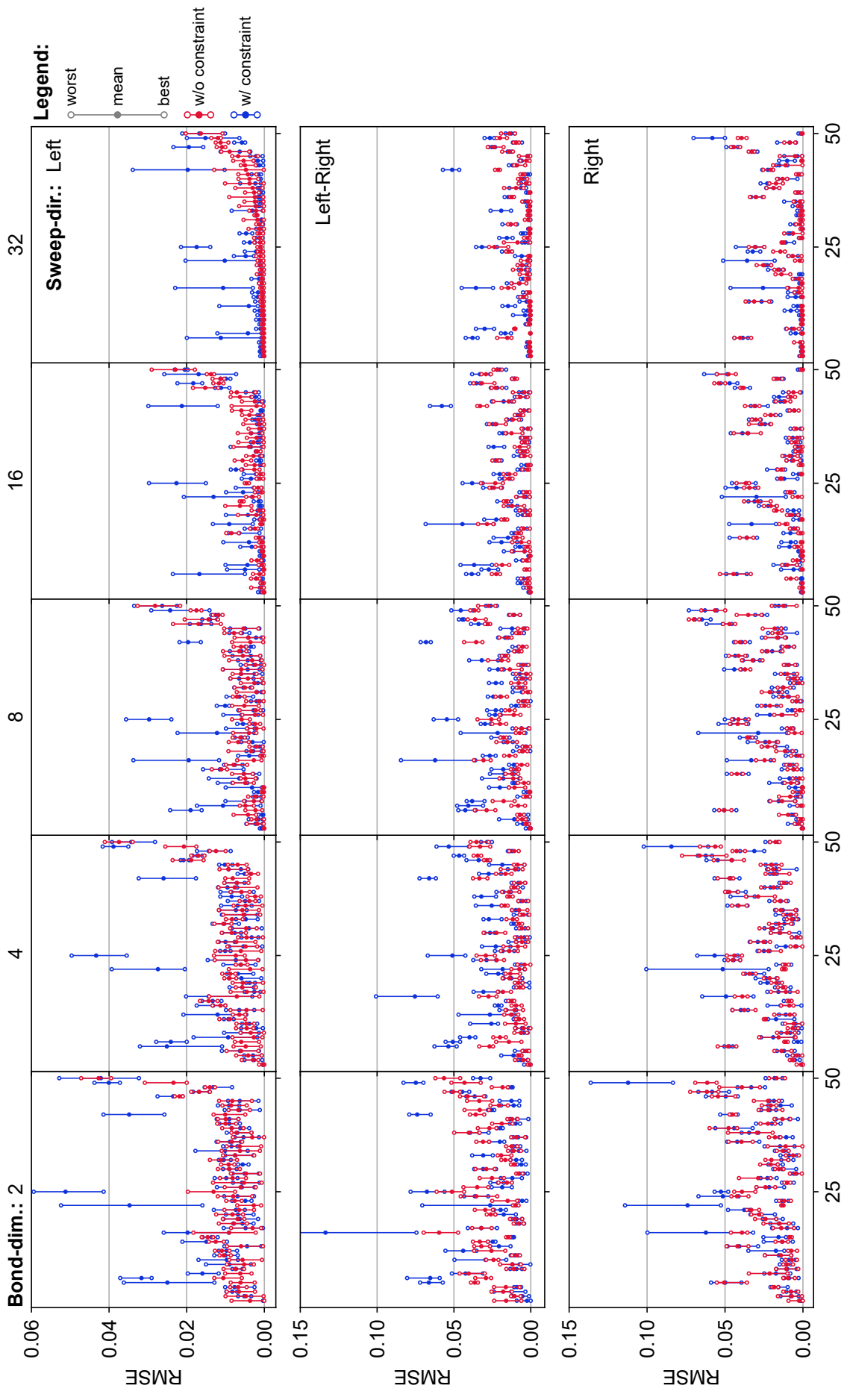


Figure 7: Summary of all DMRG samples organized in a tabular format. Rows correspond to different sweep directions (left, alternating, right) and columns represent the bond dimensions ranging from 2 to 32. For each sample, the best, worst, and average results are shown. The samples are sorted by the average values for bond dimension 32 and sweep direction left, without the constraint (top right).

References

- [1] Jingqiao Zhang and A. C. (Arthur C.) Sanderson. *Computational Intelligence in Expensive Optimization Problems*. Ed. by Yoel Tenne and Chi-Keong Goh. Vol. 2. Springer Berlin Heidelberg, 2010, p. 164. ISBN: 978-3-642-10700-9. DOI: 10.1007/978-3-642-10701-6.
- [2] Rajkumar Roy, Srichand Hinduja, and Roberto Teti. “Recent advances in engineering design optimisation: Challenges and future trends”. In: *CIRP Annals* 57 (2 2008), pp. 697–715. ISSN: 00078506. DOI: 10.1016/j.cirp.2008.09.007.
- [3] Richard M. Karp. “Reducibility among Combinatorial Problems”. In: Springer US, 1972, pp. 85–103. DOI: 10.1007/978-1-4684-2001-2_9.
- [4] Sukhpal Singh Gill et al. “Quantum computing: A taxonomy, systematic review and future directions”. In: *Software: Practice and Experience* 52 (1 Jan. 2022), pp. 66–114. ISSN: 0038-0644. DOI: 10.1002/spe.3039.
- [5] Yang Lu et al. “Quantum computing and industrial information integration: A review”. In: *Journal of Industrial Information Integration* 35 (Oct. 2023), p. 100511. ISSN: 2452414X. DOI: 10.1016/j.jii.2023.100511.
- [6] “Evidence for the utility of quantum computing before fault tolerance”. In: *Nature* 618 (7965 June 2023), pp. 500–505. ISSN: 0028-0836. DOI: 10.1038/s41586-023-06096-3.
- [7] Michael A. Nielsen and Isaac L. Chuang. *Quantum Computation and Quantum Information*. Cambridge University Press, June 2012. ISBN: 9781107002173. DOI: 10.1017/CBO9780511976667.
- [8] Richard P. Feynman. “Simulating physics with computers”. In: *International Journal of Theoretical Physics* 21 (6-7 June 1982), pp. 467–488. ISSN: 0020-7748. DOI: 10.1007/BF02650179.
- [9] Emily Grumbling and Mark Horowitz, eds. *Quantum Computing*. National Academies Press, Mar. 2019. ISBN: 978-0-309-47969-1. DOI: 10.17226/25196.
- [10] Akshay Ajagekar and Fengqi You. “Quantum computing for energy systems optimization: Challenges and opportunities”. In: *Energy* 179 (July 2019), pp. 76–89. ISSN: 03605442. DOI: 10.1016/j.energy.2019.04.186.
- [11] Eneko Osaba, Esther Villar-Rodriguez, and Izaskun Oregi. “A Systematic Literature Review of Quantum Computing for Routing Problems”. In: *IEEE Access* 10 (2022), pp. 55805–55817. ISSN: 2169-3536. DOI: 10.1109/ACCESS.2022.3177790.
- [12] Naeimeh Mohseni, Peter L. McMahon, and Tim Byrnes. “Ising machines as hardware solvers of combinatorial optimization problems”. In: *Nature Reviews Physics* 4 (6 May 2022), pp. 363–379. ISSN: 2522-5820. DOI: 10.1038/s42254-022-00440-8.
- [13] Daniel J. Egger et al. “Quantum Computing for Finance: State-of-the-Art and Future Prospects”. In: *IEEE Transactions on Quantum Engineering* 1 (2020), pp. 1–24. ISSN: 2689-1808. DOI: 10.1109/TQE.2020.3030314.
- [14] Dylan Herman et al. “A Survey of Quantum Computing for Finance”. In: *Arxiv* (Jan. 2022). arXiv: 2201.02773. URL: <http://arxiv.org/abs/2201.02773>.
- [15] Sam McArdle et al. “Quantum computational chemistry”. In: *Reviews of Modern Physics* 92 (1 Mar. 2020), p. 015003. ISSN: 0034-6861. DOI: 10.1103/RevModPhys.92.015003.
- [16] Hari P. Paudel et al. “Quantum Computing and Simulations for Energy Applications: Review and Perspective”. In: *ACS Engineering Au* 2 (3 June 2022), pp. 151–196. ISSN: 2694-2488. DOI: 10.1021/acsengineeringau.1c00033.
- [17] Annarita Giani and Zachary Eldredge. “Quantum Computing Opportunities in Renewable Energy”. In: *SN Computer Science* 2 (5 Sept. 2021), p. 393. ISSN: 2662-995X. DOI: 10.1007/s42979-021-00786-3.
- [18] Bela Bauer et al. “Quantum Algorithms for Quantum Chemistry and Quantum Materials Science”. In: *Chemical Reviews* 120 (22 Nov. 2020), pp. 12685–12717. ISSN: 0009-2665. DOI: 10.1021/acs.chemrev.9b00829.
- [19] Martin P Andersson et al. “Quantum computing for chemical and biomolecular product design”. In: *Current Opinion in Chemical Engineering* 36 (June 2022), p. 100754. ISSN: 22113398. DOI: 10.1016/j.coche.2021.100754.

[20] Hongbin Liu et al. "Prospects of quantum computing for molecular sciences". In: *Materials Theory* 6 (1 Mar. 2022), p. 11. ISSN: 2509-8012. DOI: 10.1186/s41313-021-00039-z.

[21] Yan Wang, Jungin E. Kim, and Krishnan Suresh. "Opportunities and Challenges of Quantum Computing for Engineering Optimization". In: *Journal of Computing and Information Science in Engineering* 23 (6 Dec. 2023). ISSN: 1530-9827. DOI: 10.1115/1.4062969.

[22] Yuri Alexeev et al. "Quantum-centric Supercomputing for Materials Science: A Perspective on Challenges and Future Directions". In: *Arxiv* (Dec. 2023). arXiv: 2312.09733. URL: <http://arxiv.org/abs/2312.09733>.

[23] Hossein Ghiasi, Damiano Pasini, and Larry Lessard. "Optimum stacking sequence design of composite materials Part I: Constant stiffness design". In: *Composite Structures* 90 (1 Sept. 2009), pp. 1–11. ISSN: 02638223. DOI: 10.1016/j.compstruct.2009.01.006.

[24] Hossein Ghiasi et al. "Optimum stacking sequence design of composite materials Part II: Variable stiffness design". In: *Composite Structures* 93 (1 Dec. 2010), pp. 1–13. ISSN: 02638223. DOI: 10.1016/j.compstruct.2010.06.001.

[25] S. Nikbakt, S. Kamarian, and M. Shakeri. "A review on optimization of composite structures Part I: Laminated composites". In: *Composite Structures* 195 (July 2018), pp. 158–185. ISSN: 02638223. DOI: 10.1016/j.compstruct.2018.03.063.

[26] S. Nikbakht, S. Kamarian, and M. Shakeri. "A review on optimization of composite structures Part II: Functionally graded materials". In: *Composite Structures* 214 (Apr. 2019), pp. 83–102. ISSN: 02638223. DOI: 10.1016/j.compstruct.2019.01.105.

[27] IBM Research. *How quantum computers could help design airplanes*. June 2023. URL: <https://research.ibm.com/blog/boeing-case-study> (visited on 11/24/2023).

[28] Bryce Fuller et al. "Approximate Solutions of Combinatorial Problems via Quantum Relaxations". In: *Arxiv* (Nov. 2021). arXiv: 2111.03167. URL: <http://arxiv.org/abs/2111.03167>.

[29] Koetsu Yamazaki. "Two-level optimization technique of composite laminate panels by genetic algorithms". In: vol. 37. American Institute of Aeronautics and Astronautics, Apr. 1996, pp. 1882–1887. DOI: 10.2514/6.1996-1539.

[30] J. Enrique Herencia, Paul M. Weaver, and Michael I. Friswell. "Optimization of Long Anisotropic Laminated Fiber Composite Panels with T-Shaped Stiffeners". In: *AIAA Journal* 45 (10 Oct. 2007), pp. 2497–2509. ISSN: 0001-1452. DOI: 10.2514/1.26321.

[31] Samuel T. IJsselmuiden et al. "Multi-step blended stacking sequence design of panel assemblies with buckling constraints". In: *Composites Part B: Engineering* 40 (4 June 2009), pp. 329–336. ISSN: 13598368. DOI: 10.1016/j.compositesb.2008.12.002.

[32] Dianzi Liu et al. "Bilevel Optimization of Blended Composite Wing Panels". In: *Journal of Aircraft* 48 (1 Jan. 2011), pp. 107–118. ISSN: 0021-8669. DOI: 10.2514/1.C000261.

[33] Dianzi Liu and Vassili V. Toropov. "A lamination parameter-based strategy for solving an integer-continuous problem arising in composite optimization". In: *Computers & Structures* 128 (Nov. 2013), pp. 170–174. ISSN: 00457949. DOI: 10.1016/j.compstruc.2013.06.003.

[34] Terence Macquart, Noud Werter, and Roeland De Breuker. "Aeroelastic Design of Blended Composite Structures Using Lamination Parameters". In: *Journal of Aircraft* 54 (2 Mar. 2017), pp. 561–571. ISSN: 0021-8669. DOI: 10.2514/1.C033859.

[35] Xiaoyang Liu, Carol A. Featherston, and David Kennedy. "Two-level layup optimization of composite laminate using lamination parameters". In: *Composite Structures* 211 (Mar. 2019), pp. 337–350. ISSN: 02638223. DOI: 10.1016/j.compstruct.2018.12.054.

[36] S. W. Tsai and N. J. Pagano. *Invariant Properties of Composite Materials*. 1968. URL: <https://apps.dtic.mil/sti/citations/AD0668761>.

[37] Mitsunori Miki and Yoshihiko Sugiyama. "Optimum design of laminated composite plates using lamination parameters". In: American Institute of Aeronautics and Astronautics, Apr. 1991. DOI: 10.2514/6.1991-971.

[38] Michael Chun-Yung Niu. *Airframe-Structural-Design*. Technical Book Co, 1988. ISBN: 962-7128-04-X.

[39] J A Bailie, R P Ley, and A Pasricha. *A summary and review of composite laminate design guidelines, NASA-19347*. 1997. URL: <https://www.abbott aerospace.com/downloads/nasa-nas1-19347-summary-and-review-of-composite-laminate-design-guidelines/>.

[40] *Composite Materials Handbook (Volume 3) MIL-HDBK-17-3F*. Department of Defense, USA, June 2002. URL: <https://www.abbott aerospace.com/downloads/mil-hdbk-17f/>.

[41] Mazen A. Albaazzan et al. “Efficient design optimization of nonconventional laminated composites using lamination parameters: A state of the art”. In: *Composite Structures* 209 (Feb. 2019), pp. 362–374. ISSN: 02638223. DOI: 10.1016/j.compstruct.2018.10.095.

[42] Y. Narita. “Layerwise optimization for the maximum fundamental frequency of laminated composite plates”. In: *Journal of Sound and Vibration* 263 (5 June 2003), pp. 1005–1016. ISSN: 0022460X. DOI: 10.1016/S0022-460X(03)00270-0.

[43] Julien van Campen and Zafer Gürdal. “Retrieving Variable Stiffness Laminates from Lamination Parameters Distribution”. In: American Institute of Aeronautics and Astronautics, May 2009. ISBN: 978-1-60086-975-4. DOI: 10.2514/6.2009-2183.

[44] Akira Todoroki and Yuichiro Terada. “Improved Fractal Branch and Bound Method for Stacking-Sequence Optimizations of Laminates”. In: *AIAA Journal* 42 (1 Jan. 2004), pp. 141–148. ISSN: 0001-1452. DOI: 10.2514/1.9038.

[45] Yuichiro Terada, Akira Todoroki, and Yoshinobu Shimamura. “Stacking Sequence Optimizations Using Fractal Branch and Bound Method for Laminated Composites”. In: *JSME International Journal Series A* 44 (4 2001), pp. 490–498. ISSN: 1344-7912. DOI: 10.1299/jjsmea.44.490.

[46] Akira Todoroki and Masato Sekishiro. “New iteration fractal branch and bound method for stacking sequence optimizations of multiple laminates”. In: *Composite Structures* 81 (3 Dec. 2007), pp. 419–426. ISSN: 02638223. DOI: 10.1016/j.compstruct.2006.09.001.

[47] Noémie Fedon et al. “A method using beam search to design the lay-ups of composite laminates with many plies”. In: *Composites Part C: Open Access* 4 (Mar. 2021), p. 100072. ISSN: 26666820. DOI: 10.1016/j.jcomc.2020.100072.

[48] Jung-Seok Kim, Chun-Gon Kim, and Chang-Sun Hong. “Optimum design of composite structures with ply drop using genetic algorithm and expert system shell”. In: *Composite Structures* 46 (2 Oct. 1999), pp. 171–187. ISSN: 02638223. DOI: 10.1016/S0263-8223(99)00052-5.

[49] Grant Soremekun et al. “Stacking sequence blending of multiple composite laminates using genetic algorithms”. In: *Composite Structures* 56 (1 Apr. 2002), pp. 53–62. ISSN: 02638223. DOI: 10.1016/S0263-8223(01)00185-4.

[50] Birna P. Kristinsdottir et al. “Optimal design of large composite panels with varying loads”. In: *Composite Structures* 51 (1 Jan. 2001), pp. 93–102. ISSN: 02638223. DOI: 10.1016/S0263-8223(00)00128-8.

[51] David B. Adams et al. “Genetic algorithm optimization and blending of composite laminates by locally reducing laminate thickness”. In: *Advances in Engineering Software* 35 (1 Jan. 2004), pp. 35–43. ISSN: 09659978. DOI: 10.1016/j.advengsoft.2003.09.001.

[52] Zelda B. Zabinsky, Mark E. Tuttle, and Charoenchai Khompatraporn. “A Case Study: Composite Structure Design Optimization”. In: Springer US, 2006, pp. 507–528. DOI: 10.1007/0-387-30927-6_21.

[53] Julien van Campen et al. “General Blending Definitions for Stacking Sequence Design of Composite Laminate Structures”. In: American Institute of Aeronautics and Astronautics, Apr. 2008. ISBN: 978-1-60086-993-8. DOI: 10.2514/6.2008-1798.

[54] Akira Todoroki and Raphael Haftka. “Lamination parameters for efficient genetic optimization of the stacking sequences of composite panels”. In: American Institute of Aeronautics and Astronautics, Sept. 1998, pp. 870–879. DOI: 10.2514/6.1998-4816.

[55] M. Autio. “Determining the real lay-up of a laminate corresponding to optimal lamination parameters by genetic search”. In: *Structural and Multidisciplinary Optimization* 20 (4 Dec. 2000), pp. 301–310. ISSN: 1615-147X. DOI: 10.1007/s001580050160.

[56] Mark Bloomfield, J. Herencia, and Paul Weaver. “Optimisation of Anisotropic Composite Plates Incorporating Non-Conventional Ply Orientations”. In: American Institute of Aeronautics and Astronautics, Apr. 2008. ISBN: 978-1-60086-993-8. DOI: 10.2514/6.2008-1918.

[57] Mark W. Bloomfield, J. Enrique Herencia, and Paul M. Weaver. “Enhanced two-level optimization of anisotropic laminated composite plates with strength and buckling constraints”. In: *Thin-Walled Structures* 47 (11 Nov. 2009), pp. 1161–1167. ISSN: 02638231. DOI: 10.1016/j.tws.2009.04.008.

[58] Mark W. Bloomfield, J. Enrique Herencia, and Paul M. Weaver. “Analysis and benchmarking of meta-heuristic techniques for lay-up optimization”. In: *Computers & Structures* 88 (5-6 Mar. 2010), pp. 272–282. ISSN: 00457949. DOI: 10.1016/j.compstruc.2009.10.007.

[59] F.-X. Irisarri et al. “Optimal design of laminated composite structures with ply drops using stacking sequence tables”. In: *Composite Structures* 107 (Jan. 2014), pp. 559–569. ISSN: 02638223. DOI: 10.1016/j.compstruct.2013.08.030.

[60] Yasser M. Meddaikar, François-Xavier Irisarri, and Mostafa M. Abdalla. “Laminate optimization of blended composite structures using a modified Shepard’s method and stacking sequence tables”. In: *Structural and Multidisciplinary Optimization* 55 (2 Feb. 2017), pp. 535–546. ISSN: 1615-147X. DOI: 10.1007/s00158-016-1508-0.

[61] Yudong Cao et al. “Quantum Chemistry in the Age of Quantum Computing”. In: *Chemical Reviews* 119 (19 Oct. 2019), pp. 10856–10915. ISSN: 0009-2665. DOI: 10.1021/acs.chemrev.8b00803.

[62] Philipp Hauke et al. “Perspectives of quantum annealing: methods and implementations”. In: *Reports on Progress in Physics* 83 (5 May 2020), p. 054401. ISSN: 0034-4885. DOI: 10.1088/1361-6633/ab85b8.

[63] A. Yu. Kitaev. “Quantum measurements and the Abelian Stabilizer Problem”. In: *Arxiv* (Nov. 1995). arXiv: quant-ph/9511026. URL: <http://arxiv.org/abs/quant-ph/9511026>.

[64] Daniel S. Abrams and Seth Lloyd. “Quantum Algorithm Providing Exponential Speed Increase for Finding Eigenvalues and Eigenvectors”. In: *Physical Review Letters* 83 (24 Dec. 1999), pp. 5162–5165. ISSN: 0031-9007. DOI: 10.1103/PhysRevLett.83.5162.

[65] Thomas Ayral et al. “Quantum computing with and for many-body physics”. In: *The European Physical Journal A* 59 (10 Oct. 2023), p. 227. ISSN: 1434-601X. DOI: 10.1140/epja/s10050-023-01141-1.

[66] Alberto Peruzzo et al. “A variational eigenvalue solver on a photonic quantum processor”. In: *Nature Communications* 5 (1 July 2014), p. 4213. ISSN: 2041-1723. DOI: 10.1038/ncomms5213.

[67] Edward Farhi, Jeffrey Goldstone, and Sam Gutmann. “A Quantum Approximate Optimization Algorithm”. In: *Arxiv* (Nov. 2014). arXiv: 1411.4028. URL: <http://arxiv.org/abs/1411.4028>.

[68] M. Cerezo et al. “Variational quantum algorithms”. In: *Nature Reviews Physics* 3 (9 Aug. 2021), pp. 625–644. ISSN: 2522-5820. DOI: 10.1038/s42254-021-00348-9.

[69] Suguru Endo et al. “Hybrid Quantum-Classical Algorithms and Quantum Error Mitigation”. In: *Journal of the Physical Society of Japan* 90 (3 Mar. 2021), p. 032001. ISSN: 0031-9015. DOI: 10.7566/JPSJ.90.032001.

[70] Tadashi Kadowaki and Hidetoshi Nishimori. “Quantum annealing in the transverse Ising model”. In: *Physical Review E* 58 (5 Nov. 1998), pp. 5355–5363. ISSN: 1063-651X. DOI: 10.1103/PhysRevE.58.5355.

[71] Tadashi Kadowaki. “Study of Optimization Problems by Quantum Annealing”. In: *Arxiv* (May 2002). arXiv: quant-ph/0205020. URL: <http://arxiv.org/abs/quant-ph/0205020>.

[72] Steven R. White. “Density matrix formulation for quantum renormalization groups”. In: *Physical Review Letters* 69 (19 Nov. 1992), pp. 2863–2866. ISSN: 0031-9007. DOI: 10.1103/PhysRevLett.69.2863.

[73] Steven R. White. “Density-matrix algorithms for quantum renormalization groups”. In: *Physical Review B* 48 (14 Oct. 1993), pp. 10345–10356. ISSN: 0163-1829. DOI: 10.1103/PhysRevB.48.10345.

[74] Tomotoshi Nishino and Kouichi Okunishi. “Corner Transfer Matrix Renormalization Group Method”. In: *Journal of the Physical Society of Japan* 65 (4 Apr. 1996), pp. 891–894. ISSN: 0031-9015. DOI: 10.1143/JPSJ.65.891.

[75] F. Verstraete, D. Porras, and J. I. Cirac. “Density Matrix Renormalization Group and Periodic Boundary Conditions: A Quantum Information Perspective”. In: *Physical Review Letters* 93 (22 Nov. 2004), p. 227205. ISSN: 0031-9007. DOI: 10.1103/PhysRevLett.93.227205.

[76] Ulrich Schollwöck. “The density-matrix renormalization group in the age of matrix product states”. In: *Annals of Physics* 326 (1 Jan. 2011), pp. 96–192. ISSN: 00034916. DOI: 10.1016/j.aop.2010.09.012.

[77] Garnet Kin-Lic Chan et al. “Matrix Product Operators, Matrix Product States, and ab initio Density Matrix Renormalization Group algorithms”. In: *Arxiv* (May 2016). arXiv: 1605.02611. URL: <http://arxiv.org/abs/1605.02611>.

[78] *Fiber Technology for Fiber-Reinforced Composites*. Elsevier, 2017. ISBN: 9780081018712. DOI: 10.1016/C2015-0-05497-1.

[79] E. Reissner and Y. Stavsky. “Bending and Stretching of Certain Types of Heterogeneous Aeolotropic Elastic Plates”. In: *Journal of Applied Mechanics* 28 (3 Sept. 1961), pp. 402–408. ISSN: 0021-8936. DOI: 10.1115/1.3641719.

[80] S. B. Dong, K. S. Pister, and R. L. Taylor. “On the Theory of Laminated Anisotropic Shells and Plates”. In: *Journal of the Aerospace Sciences* 29 (8 Aug. 1962), pp. 969–975. ISSN: 1936-9999. DOI: 10.2514/8.9668.

[81] Stephen W. Tsai and H. Thomas Hahn. *Introduction to Composite Materials*. Routledge, Oct. 1980. ISBN: 9780203750148. DOI: 10.1201/9780203750148.

[82] Samuel T. IJsselmuiden. “Optimal Design of Variable Stiffness Composite Structures Using Lamination Parameters”. In: (2011). URL: <http://resolver.tudelft.nl/uuid:973a564b-5734-42c4-a67c-1044f1e25f1c>.

[83] Moritz Sprengholz et al. “Rapid transformation of lamination parameters into stacking sequences”. In: *Composite Structures* 276 (Nov. 2021), p. 114514. ISSN: 02638223. DOI: 10.1016/j.compstruct.2021.114514.

[84] Michele Mosca. “Quantum Algorithms”. In: *Arxiv* (Aug. 2008). arXiv: 0808.0369. URL: <http://arxiv.org/abs/0808.0369>.

[85] Ashley Montanaro. “Quantum algorithms: an overview”. In: *npj Quantum Information* 2 (1 Jan. 2016), p. 15023. ISSN: 2056-6387. DOI: 10.1038/npjqi.2015.23.

[86] Kishor Bharti et al. “Noisy intermediate-scale quantum algorithms”. In: *Reviews of Modern Physics* 94 (1 Feb. 2022), p. 015004. ISSN: 0034-6861. DOI: 10.1103/RevModPhys.94.015004.

[87] G. Ntourmas et al. “Mixed Integer Linear Programming formulations of the stacking sequence and blending optimisation of composite structures”. In: *Composite Structures* 264 (May 2021), p. 113660. ISSN: 02638223. DOI: 10.1016/j.compstruct.2021.113660.

[88] P. Jordan and E. Wigner. “Über das Paulische Äquivalenzverbot”. In: *Zeitschrift für Physik* 47 (9-10 Sept. 1928), pp. 631–651. ISSN: 1434-6001. DOI: 10.1007/BF01331938.

[89] Daniel S. Abrams and Seth Lloyd. “Simulation of Many-Body Fermi Systems on a Universal Quantum Computer”. In: *Physical Review Letters* 79 (13 Sept. 1997), pp. 2586–2589. ISSN: 0031-9007. DOI: 10.1103/PhysRevLett.79.2586.

[90] Sergey B. Bravyi and Alexei Yu. Kitaev. “Fermionic Quantum Computation”. In: *Annals of Physics* 298 (1 May 2002), pp. 210–226. ISSN: 00034916. DOI: 10.1006/aphy.2002.6254.

[91] Jacob T. Seeley, Martin J. Richard, and Peter J. Love. “The Bravyi-Kitaev transformation for quantum computation of electronic structure”. In: *The Journal of Chemical Physics* 137 (22 Dec. 2012). ISSN: 0021-9606. DOI: 10.1063/1.4768229.

[92] Hartmut Neven, Geordie Rose, and William G. Macready. “Image recognition with an adiabatic quantum computer I. Mapping to quadratic unconstrained binary optimization”. In: *Arxiv* (Apr. 2008). arXiv: 0804.4457. URL: <http://arxiv.org/abs/0804.4457>.

[93] Zhengbing Bian et al. *The Ising model: teaching an old problem new tricks*. 2010. URL: <https://www.dwavesys.com/resources/publication/the-ising-model-teaching-an-old-problem-new-tricks/>.

[94] Eleanor G. Rieffel et al. “A case study in programming a quantum annealer for hard operational planning problems”. In: *Quantum Information Processing* 14 (1 Jan. 2015), pp. 1–36. ISSN: 1570-0755. DOI: 10.1007/s11128-014-0892-x.

[95] Alexandre Blais et al. “Circuit quantum electrodynamics”. In: *Arxiv* 93 (2 May 2021), p. 025005. ISSN: 0034-6861. DOI: 10.1103/RevModPhys.93.025005. arXiv: 2005.12667.

[96] Colin D. Bruzewicz et al. “Trapped-ion quantum computing: Progress and challenges”. In: *Arxiv* 6 (2 June 2019). ISSN: 1931-9401. DOI: 10.1063/1.5088164. arXiv: 1904.04178.

[97] “Quantum approximate optimization of the long-range Ising model with a trapped-ion quantum simulator”. In: *Proceedings of the National Academy of Sciences* 117 (41 Oct. 2020), pp. 25396–25401. ISSN: 0027-8424. DOI: 10.1073/pnas.2006373117.

[98] “Logical quantum processor based on reconfigurable atom arrays”. In: *Nature* (Dec. 2023). ISSN: 0028-0836. DOI: 10.1038/s41586-023-06927-3.

[99] Thomas Gabor et al. “How to Approximate any Objective Function via Quadratic Unconstrained Binary Optimization”. In: IEEE, Mar. 2022, pp. 1249–1257. ISBN: 978-1-6654-3786-8. DOI: 10.1109/SANER53432.2022.00149.

[100] Gary Kochenberger et al. “The unconstrained binary quadratic programming problem: a survey”. In: *Journal of Combinatorial Optimization* 28 (1 July 2014), pp. 58–81. ISSN: 1382-6905. DOI: 10.1007/s10878-014-9734-0.

[101] Andrew Lucas. “Ising formulations of many NP problems”. In: *Frontiers in Physics* 2 (2014), pp. 1–14. ISSN: 2296-424X. DOI: 10.3389/fphy.2014.00005.

[102] Itay Hen and Federico M. Spedalieri. “Quantum Annealing for Constrained Optimization”. In: *Physical Review Applied* 5 (3 Mar. 2016), p. 034007. ISSN: 2331-7019. DOI: 10.1103/PhysRevApplied.5.034007.

[103] Fred Glover et al. “Quantum bridge analytics I: a tutorial on formulating and using QUBO models”. In: *Annals of Operations Research* 314 (1 July 2022), pp. 141–183. ISSN: 0254-5330. DOI: 10.1007/s10479-022-04634-2.

[104] John Parkinson and Damian J J Farnell. *An Introduction to Quantum Spin Systems*. Vol. 816. Springer Berlin Heidelberg, 2010. ISBN: 978-3-642-13289-6. DOI: 10.1007/978-3-642-13290-2.

[105] John B. Kogut. “An introduction to lattice gauge theory and spin systems”. In: *Reviews of Modern Physics* 51 (4 Oct. 1979), pp. 659–713. ISSN: 0034-6861. DOI: 10.1103/RevModPhys.51.659.

[106] David Poulin and Paweł Wocjan. “Preparing Ground States of Quantum Many-Body Systems on a Quantum Computer”. In: *Physical Review Letters* 102 (13 Apr. 2009), p. 130503. ISSN: 0031-9007. DOI: 10.1103/PhysRevLett.102.130503.

[107] J. Eisert, M. Cramer, and M. B. Plenio. “Colloquium : Area laws for the entanglement entropy”. In: *Reviews of Modern Physics* 82 (1 Feb. 2010), pp. 277–306. ISSN: 0034-6861. DOI: 10.1103/RevModPhys.82.277.

[108] Alba Cervera-Lierta. “Exact Ising model simulation on a quantum computer”. In: *Quantum* 2 (Dec. 2018), p. 114. ISSN: 2521-327X. DOI: 10.22331/q-2018-12-21-114.

[109] I G Rosenberg. “Reduction of bivalent maximization to the quadratic case”. In: *Cahiers du Centre d’Études de Recherche Opérationnelle* 17 (1975), pp. 71–74.

[110] Martin Anthony et al. “Quadratic reformulations of nonlinear binary optimization problems”. In: *Mathematical Programming* 162 (1-2 Mar. 2017), pp. 115–144. ISSN: 0025-5610. DOI: 10.1007/s10107-016-1032-4.

[111] Nike Dattani. “Quadratization in discrete optimization and quantum mechanics”. In: *Arxiv* (Jan. 2019). arXiv: 1901.04405. URL: <http://arxiv.org/abs/1901.04405>.

[112] Endre Boros, Yves Crama, and Elisabeth Rodríguez-Heck. “Compact quadratizations for pseudo-Boolean functions”. In: *Journal of Combinatorial Optimization* 39 (3 Apr. 2020), pp. 687–707. ISSN: 1382-6905. DOI: 10.1007/s10878-019-00511-0.

[113] John Preskill. “Quantum Computing in the NISQ era and beyond”. In: *Quantum* 2 (Aug. 2018), p. 79. ISSN: 2521-327X. DOI: 10.22331/q-2018-08-06-79.

[114] J Dukelsky et al. “Equivalence of the variational matrix product method and the density matrix renormalization group applied to spin chains”. In: *Europhysics Letters (EPL)* 43 (4 Aug. 1998), pp. 457–462. ISSN: 0295-5075. DOI: 10.1209/epl/i1998-00381-x.

[115] Roger Penrose. “Applications of negative dimensional tensors”. In: Academic Press, London, 1971, pp. 221–244.

[116] Román Orús. “A practical introduction to tensor networks: Matrix product states and projected entangled pair states”. In: *Annals of Physics* 349 (Oct. 2014), pp. 117–158. ISSN: 00034916. DOI: 10.1016/j.aop.2014.06.013.

[117] Román Orús. “Tensor networks for complex quantum systems”. In: *Nature Reviews Physics* 1 (9 Aug. 2019), pp. 538–550. ISSN: 2522-5820. DOI: 10.1038/s42254-019-0086-7.

[118] Jacob C Bridgeman and Christopher T Chubb. “Hand-waving and interpretive dance: an introductory course on tensor networks”. In: *Journal of Physics A: Mathematical and Theoretical* 50 (22 June 2017), p. 223001. ISSN: 1751-8113. DOI: 10.1088/1751-8121/aa6dc3.

[119] Jacob Biamonte and Ville Bergholm. “Tensor Networks in a Nutshell”. In: *Arxiv* (July 2017). arXiv: 1708.00006. URL: <http://arxiv.org/abs/1708.00006>.

[120] J. Ignacio Cirac et al. “Matrix product states and projected entangled pair states: Concepts, symmetries, theorems”. In: *Reviews of Modern Physics* 93 (4 Dec. 2021), p. 045003. ISSN: 0034-6861. DOI: 10.1103/RevModPhys.93.045003.

[121] Glen Evenbly. “A Practical Guide to the Numerical Implementation of Tensor Networks I: Contractions, Decompositions and Gauge Freedom”. In: *Arxiv* (Feb. 2022). arXiv: 2202.02138. URL: <http://arxiv.org/abs/2202.02138>.

[122] M.B. Plenio and S. Virmani. “An introduction to entanglement measures”. In: *Arxiv* 7 (1&2 Jan. 2007), pp. 1–51. ISSN: 15337146. DOI: 10.26421/QIC7.1-2-1. arXiv: quant-ph/0504163.

[123] Ryszard Horodecki et al. “Quantum entanglement”. In: *Reviews of Modern Physics* 81 (2 June 2009), pp. 865–942. ISSN: 0034-6861. DOI: 10.1103/RevModPhys.81.865.

[124] J I Latorre and A Riera. “A short review on entanglement in quantum spin systems”. In: *Journal of Physics A: Mathematical and Theoretical* 42 (50 Dec. 2009), p. 504002. ISSN: 1751-8113. DOI: 10.1088/1751-8113/42/50/504002.

[125] Nicolas Laflorencie. “Quantum entanglement in condensed matter systems”. In: *Physics Reports* 646 (Aug. 2016), pp. 1–59. ISSN: 03701573. DOI: 10.1016/j.physrep.2016.06.008.

[126] Guifré Vidal. “Efficient Classical Simulation of Slightly Entangled Quantum Computations”. In: *Physical Review Letters* 91 (14 Oct. 2003), p. 147902. ISSN: 0031-9007. DOI: 10.1103/PhysRevLett.91.147902.

[127] Guifré Vidal. “Efficient Simulation of One-Dimensional Quantum Many-Body Systems”. In: *Physical Review Letters* 93 (4 July 2004), p. 040502. ISSN: 0031-9007. DOI: 10.1103/PhysRevLett.93.040502.

[128] Sebastian Paeckel et al. “Time-evolution methods for matrix-product states”. In: *Annals of Physics* 411 (Dec. 2019), p. 167998. ISSN: 00034916. DOI: 10.1016/j.aop.2019.167998.

[129] F. Verstraete and J. I. Cirac. “Matrix product states represent ground states faithfully”. In: *Physical Review B* 73 (9 Mar. 2006), p. 094423. ISSN: 1098-0121. DOI: 10.1103/PhysRevB.73.094423.

[130] M B Hastings. “An area law for one-dimensional quantum systems”. In: *Journal of Statistical Mechanics: Theory and Experiment* 2007 (08 Aug. 2007), P08024–P08024. ISSN: 1742-5468. DOI: 10.1088/1742-5468/2007/08/P08024.

[131] C. Hubig, I. P. McCulloch, and U. Schollwöck. “Generic construction of efficient matrix product operators”. In: *Physical Review B* 95 (3 Jan. 2017), p. 035129. ISSN: 2469-9950. DOI: 10.1103/PhysRevB.95.035129.

[132] Daniel E. Parker, Xiangyu Cao, and Michael P. Zaletel. “Local matrix product operators: Canonical form, compression, and control theory”. In: *Physical Review B* 102 (3 July 2020), p. 035147. ISSN: 2469-9950. DOI: 10.1103/PhysRevB.102.035147.

[133] C. Lanczos. “An iteration method for the solution of the eigenvalue problem of linear differential and integral operators”. In: *Journal of Research of the National Bureau of Standards* 45 (4 Oct. 1950), p. 255. ISSN: 0091-0635. DOI: 10.6028/jres.045.026.

[134] C. C. Paige. “Computational Variants of the Lanczos Method for the Eigenproblem”. In: *IMA Journal of Applied Mathematics* 10 (3 1972), pp. 373–381. ISSN: 0272-4960. DOI: 10.1093/imamat/10.3.373.

[135] Ian P McCulloch. “From density-matrix renormalization group to matrix product states”. In: *Journal of Statistical Mechanics: Theory and Experiment* 2007 (10 Oct. 2007), P10014–P10014. ISSN: 1742-5468. DOI: 10.1088/1742-5468/2007/10/P10014.

[136] Matthew Fishman, Steven R. White, and E. Miles Stoudenmire. “The ITensor Software Library for Tensor Network Calculations”. In: *SciPost Phys. Codebases* (2022), p. 4. DOI: 10.21468/SciPostPhysCodeb.4.

[137] Matthew Fishman, Steven R. White, and E. Miles Stoudenmire. "Codebase release 0.3 for ITensor". In: *SciPost Phys. Codebases* (2022), 4-r0.3. DOI: 10.21468/SciPostPhysCodeb.4-r0.3.

[138] Arne Wulff et al. *Research Code Accompanying the Publication: "Quantum Computing and Tensor Networks for Laminate Design: A Novel Approach to Stacking Sequence Retrieval"*. 2024. URL: <https://github.com/ArneWulff/stacking-sequence-retrieval-with-dmrg>.

[139] Arne Wulff et al. *Research Data Accompanying the Publication: "Quantum Computing and Tensor Networks for Laminate Design: A Novel Approach to Stacking Sequence Retrieval"*. 2024. DOI: 10.4121/ae276609-55b0-4af1-88c0-1102b1b58990.

[140] George Marsh. "Aero engines lose weight thanks to composites". In: *Reinforced Plastics* 56 (6 Nov. 2012), pp. 32–35. ISSN: 00343617. DOI: 10.1016/S0034-3617(12)70146-7.

[141] Niels van Hoorn, Christos Kassapoglou, and Wouter Brink. "Impact response of thick composite structures". In: *6th ECCOMAS Thematic Conference on the Mechanical Response of Composites*. Sept. 2017. URL: https://pure.tudelft.nl/ws/portalfiles/portal/31278049/Hoorn_full_paper_composites2017.pdf.

[142] Matthew J. Donough et al. "In-Plane and Oblique Edge-on Impact on Thick Glass-Fibre/Epoxy Composite Laminates". In: *International Journal of Impact Engineering* 171 (Jan. 2023), p. 104373. ISSN: 0734743X. DOI: 10.1016/j.ijimpeng.2022.104373.

[143] Murray Rosenblatt. "Remarks on Some Nonparametric Estimates of a Density Function". In: *The Annals of Mathematical Statistics* 27 (3 Sept. 1956), pp. 832–837. ISSN: 0003-4851. DOI: 10.1214/aoms/1177728190.

[144] Emanuel Parzen. "On Estimation of a Probability Density Function and Mode". In: *The Annals of Mathematical Statistics* 33 (3 Sept. 1962), pp. 1065–1076. ISSN: 0003-4851. DOI: 10.1214/aoms/1177704472.

[145] Stanisław Weglarczyk. "Kernel density estimation and its application". In: *ITM Web of Conferences* 23 (Nov. 2018). Ed. by W. Zielinski et al., p. 00037. ISSN: 2271-2097. DOI: 10.1051/itmconf/20182300037.

[146] Shi-Ju Ran. "Encoding of matrix product states into quantum circuits of one- and two-qubit gates". In: *Physical Review A* 101 (3 Mar. 2020), p. 032310. ISSN: 2469-9926. DOI: 10.1103/PhysRevA.101.032310.

[147] Manuel S. Rudolph et al. "Decomposition of Matrix Product States into Shallow Quantum Circuits". In: *Arxiv* (Sept. 2022). arXiv: 2209.00595. URL: <http://arxiv.org/abs/2209.00595>.

[148] Daniel Malz et al. "Preparation of Matrix Product States with Log-Depth Quantum Circuits". In: *Physical Review Letters* 132 (4 Jan. 2024), p. 040404. ISSN: 0031-9007. DOI: 10.1103/PhysRevLett.132.040404.

[149] Manuel S. Rudolph et al. "Synergy Between Quantum Circuits and Tensor Networks: Short-cutting the Race to Practical Quantum Advantage". In: *Arxiv* (Aug. 2022). arXiv: 2208.13673. URL: <http://arxiv.org/abs/2208.13673>.

[150] Jarrod R. McClean et al. "Barren plateaus in quantum neural network training landscapes". In: *Nature Communications* 9 (1 Nov. 2018), p. 4812. ISSN: 2041-1723. DOI: 10.1038/s41467-018-07090-4.

[151] Lennart Bittel and Martin Kliesch. "Training Variational Quantum Algorithms Is NP-Hard". In: *Physical Review Letters* 127 (12 Sept. 2021), p. 120502. ISSN: 0031-9007. DOI: 10.1103/PhysRevLett.127.120502.

[152] Chufan Lyu, Victor Montenegro, and Abolfazl Bayat. "Accelerated variational algorithms for digital quantum simulation of many-body ground states". In: *Quantum* 4 (Sept. 2020), p. 324. ISSN: 2521-327X. DOI: 10.22331/q-2020-09-16-324.

[153] Andrea Skolik et al. "Layerwise learning for quantum neural networks". In: *Quantum Machine Intelligence* 3 (1 June 2021), p. 5. ISSN: 2524-4906. DOI: 10.1007/s42484-020-00036-4.

[154] Leo Zhou et al. "Quantum Approximate Optimization Algorithm: Performance, Mechanism, and Implementation on Near-Term Devices". In: *Physical Review X* 10 (2 June 2020), p. 021067. ISSN: 2160-3308. DOI: 10.1103/PhysRevX.10.021067.

- [155] Edward Grant et al. “An initialization strategy for addressing barren plateaus in parametrized quantum circuits”. In: *Quantum* 3 (Dec. 2019), p. 214. ISSN: 2521-327X. DOI: 10.22331/q-2019-12-09-214.
- [156] Guillaume Verdon et al. “Learning to learn with quantum neural networks via classical neural networks”. In: *Arxiv* (July 2019). arXiv: 1907.05415. URL: <http://arxiv.org/abs/1907.05415>.
- [157] Daniel J. Egger, Jakub Mareček, and Stefan Woerner. “Warm-starting quantum optimization”. In: *Quantum* 5 (June 2021), p. 479. ISSN: 2521-327X. DOI: 10.22331/q-2021-06-17-479.
- [158] Felix Truger et al. “Warm-Starting and Quantum Computing: A Systematic Mapping Study”. In: *Arxiv* (Mar. 2023). arXiv: 2303.06133. URL: <http://arxiv.org/abs/2303.06133>.
- [159] Y.-Y. Shi, L.-M. Duan, and G. Vidal. “Classical simulation of quantum many-body systems with a tree tensor network”. In: *Physical Review A* 74 (2 Aug. 2006), p. 022320. ISSN: 1050-2947. DOI: 10.1103/PhysRevA.74.022320.
- [160] G. Vidal. “Entanglement Renormalization”. In: *Physical Review Letters* 99 (22 Nov. 2007), p. 220405. ISSN: 0031-9007. DOI: 10.1103/PhysRevLett.99.220405.
- [161] Boyang Liu et al. “Permutation genetic algorithm for stacking sequence design of composite laminates”. In: *Computer Methods in Applied Mechanics and Engineering* 186 (2-4 June 2000), pp. 357–372. ISSN: 00457825. DOI: 10.1016/S0045-7825(99)90391-2.
- [162] Peter C. Fishburn. “Letter to the Editor—Additive Utilities with Incomplete Product Sets: Application to Priorities and Assignments”. In: *Operations Research* 15 (3 June 1967), pp. 537–542. ISSN: 0030-364X. DOI: 10.1287/opre.15.3.537.
- [163] C. West Churchman and Russell L. Ackoff. “An Approximate Measure of Value”. In: *Journal of the Operations Research Society of America* 2 (2 May 1954), pp. 172–187. ISSN: 0096-3984. DOI: 10.1287/opre.2.2.172.
- [164] JosÉ Figueira, Salvatore Greco, and Matthias Ehrgott. *Multiple Criteria Decision Analysis: State of the Art Surveys*. Vol. 78. Springer New York, 2005. ISBN: 978-0-387-23067-2. DOI: 10.1007/b100605.